Conceptual design report

Individual Radioactive Ion Injection, Cooling and Storage in a Ring

I.Meshkov[1], W.Mitting[2], P.Roussel-Chomaz[2], A.Sidorin[1], A.Smirnov[1], E. Syresin[1],

JINR[1]/GANIL[2] Collaboration

JINR/GANIL

Dubna

2002

Contents

1. Introduction

A radioactive ion beam (RIB) produced at a target bombarded with a primary beam has after a fragment separator usually a large emittance of $\varepsilon \approx 200\pi$ ·mm·mrad. We consider here the typical parameters for a radioactive ion accelerator facility with a quasi-continuous ion flux from an ion accelerator at the particle energy about 0.5 ÷ 1 GeV/u. (Table 1.1) [1]. These parameters can be realised at slow primary beam extraction from a synchrotron, for example, from SIS at GSI [2], or from a high energy cyclotrons, like cyclotron complex under construction at RIKEN [3].

Number of the ions N stored in a ring is determined by storage rate R_{store} and the ion life time τ_{life} and can be estimated as follows:

$$N \sim R_{store}\tau_{life}. \tag{1.1}$$

Thus, for experiments with short lived isotopes one need to provide maximum value of the storage rate. The storage rate is determined by the ion number injected during single injection cycle N_{inj} and period of time required for displacement of the injected ions to the stack τ_{st}:

$$R_{store} = \eta_{st} \cdot N_{inj}/\tau_{st}, \tag{1.2}$$

where η_{st} is the stacking procedure efficiency.

Several schemes of the storage ring were proposed to provide a high storage rate of the ions at relatively pure ion flux $\hat{N}_i$ from the fragment separator. For instance, at ACR ring of the MUSES project one plans to perform multiturn injection and ion storage in the longitudinal phase space. In this case the ion number injected during single injection cycle is determined by the ion turn number at the injection n_{turn}:

$$N_{inj} = \eta_{mt} \hat{N}_i n_{turn} T_{rev}, \tag{1.3}$$

where η_{mt} is the efficiency of the multiturn injection and T_{rev} is the ion revolution period in the ring. The stacking procedure includes stochastic cooling of the injected ions, bunching and RF stacking. The stacking time can be estimated as a sum of the cooling time τ_{cool} and time of the bunching and RF stacking τ_{RF}:

$$\tau_{st} = \tau_{cool} + \tau_{RF}. \tag{1.4}$$

Finally, the storage rate at this scheme can be estimated as:

$$R_{store} = \eta_{mt}\eta_{stack} \frac{\hat{N}_i n_{turn} T_{rev}}{\tau_{st}}. \tag{1.5}$$

At typical parameters of the storage ring and stacking process

$$n_{inj} \sim 15\text{-}20,\ T_{rev} \sim 1\ \mu s,\ \tau_{st}\ \text{is about a few hundreds of ms},\ \eta_{mt}\eta_{stack} \sim 0.5 \tag{1.6}$$

the storage rate is of the order of $10^{-5} \cdot \hat{N}_i$ and exceeds 10^3 ions/s at the ion flux of 10^8 ions/s.

This scheme requires a large transverse and longitudinal acceptance of the ring and it can work at sufficiently large ion flux only. In reality, at continuos ion flux the number of injected ions (formula 1.3) is sufficiently larger than unit only at flux intensity higher than 10^6 ions/s. At flux intensity of 10^5 ions/s a few ions will be injected during injection period only, and at the flux intensity below 10^5 ions/s a single ion will be stored during several stacking procedures. Correspondingly, for RIB at small production rate - from 10^5 ions/s down to 1 ion/s the efficiency of this scheme does not allow to store in the ring an ion number required for experiment. The situation can be improved by time modulation of the ion flux from the fragment separator, however this leads to target operation at a higher peak power of the primary beam.

Table 1.1. Parameters of the RIB

Ion energy, MeV/u	700
Ion charge number Z	50
Atomic mass number A	132
RIB intensity, s^{-1}	$1 \div 10^6$
Beam emittance, $\pi \cdot$mm· mrad	200
Beam size, mm	$\pm 3{,}5$
Angular spread, mrad	± 50
Momentum spread, $\Delta p / p$	$\pm 2{,}5 \cdot 10^{-2}$
Coordinate resolution, Δx, Δy, mm	$\pm 0{,}2$
Angular resolution, $\Delta\theta$, $\Delta\varphi$, mrad	± 1 mrad
Time resolution, ns	$\pm 0{,}1$
Momentum resolution, $\delta p / p$	$\pm 5 \cdot 10^{-4}$

Here we discuss an alternative storage scheme recently proposed [1], which is oriented to the continuos ion beam from fragment separator at *production rate of 10^4 ions/s or even les*s.

At low production rate the parameters of each particle can be measured individually with rather high accuracy. Assuming the resolution presented in Table 1.1 is achievable we see that "individual emittance" of each particle is very low - of the order of

$$\varepsilon_{ind} \approx 0{,}2\pi \cdot mm \cdot mrad \,, \qquad (1.7)$$

which is less than total beam emittance by three order of magnitudes. Using a system of kickers in the ion transportation channel (transfer channel) from the fragment separator to the injection point one can compensate initial ion co-ordinate and angle of the ion and inject into the ring a beam at emittance closed to "individual" one (see Sections 3.2, 3.5). Initial momentum shift of every ion can be reduced with a profile energy degrader (see Section 3.4). For such a scheme maximum ion flux is limited by a technically achievable repetition frequency of the kickers operation. At required kicker voltage (see Section 3.2) this value can be estimated as 10 kHz approximately.

Knowing the moment of the ion born at the target one can provide an "individual injection" of the ion into the ring. The injection is performed by a fast kicker controlled by the signal from

analyser system at the exit of fragment separator. To avoid losses of ions stacked before the stored beam has to be bunched and the bunch length has to be sufficiently less than the ring circumference. In this case the injection kicker operation can be synchronised with the bunch revolution. The number of injected particles during single injection cycle is determined by the cycle duration, which can be sufficiently longer than in the scheme with multiturn injection (formula 1.3). As it will be shown in the section 5 this scheme allows to inject into the ring $10 \div 20$ ions during an injection cycle of a few ms duration.

Small values of the emittance and momentum spread of the injected beam allow to reduce the stacking time to the value of about 30 ms (Section 6). The stacking can be performed using a conventional electron cooling system in combination with induction acceleration of the ions (Section 6.1), or an electron cooling system with gradient of the longitudinal electron velocity (Section 6.2). An application of stochastic cooling for the stacking is possible also and it is discussed in the Section 6.3.

Thus, using the "individual trajectory correction" in the transfer channel, "individual injection" in the storage ring and fast stacking procedure applied for injected beam at small emittance and momentum spread one can obtain a storage rate of $10^2 \div 10^3$ ions/s at ion flux of 10^4 ions/s or less. This scheme does not require a storage ring of a large acceptance. In principle, the proposed design of the transfer channel can be used for the beam emittance and momentum spread reduction in an experiment with an external target as well.

2. General description

The technical questions related to a fast staking procedure of a large emittance beam with well-measured particle parameters (Table 1) [1] are discussed in this paper. The proposed facility has the following features.

1) The transfer channel from the fragment separator to the storage ring includes kickers which parameters are adjusted for every individual particle. The channel has a large acceptance ($\approx 200\pi \cdot mm \cdot mrad$) and contains

- a pair of kickers used for correction of particle angular deviation and spatial transverse displacement relatively to equilibrium trajectory for each transverse direction: horizontal *x* and vertical *y*,
- a profiled degrader applied for reduction of the ion momentum spread,
- second pair of kickers correcting a distortion of the particle trajectory due to action of the degrader.

The application of the profiled degrader and two pairs of kickers permits to reduce the particle momentum spread to $\Delta p/p = \pm 2.5 \cdot 10^{-3}$ and the particle flux emittance to $1.5\ \pi \cdot mm \cdot mrad$. In this case the acceptance of storage ring may be relatively small of 5-10 $\pi \cdot mm \cdot mrad$ and as the result electron cooling is fast.

2) Individual injection of every particle into the ring is used. Contrary to conventional injection in a standard synchrotron one can not provide in this case a synchronisation between the stored stack and a new injected particle that is caused by a random character of radioactive ion production. As result, several tens of new injected particles circulate in the ring out of the stack occupying the ring orbit if typical injection repetition period is smaller than particle cooling time. It limits particle injection rate. However, one can synchronize the injection kicker operation with the stack and the particles, which are not stacked yet and circulate in the ring. It can be done if the ring operates near the transition energy (see details in the Section 4.2).

3) Stacking of the ion beam inside the storage ring is provided in the longitudinal phase space. The momentum of the new injected particle is shifted by some value from the momentum of the stack particles. The reduction of the momentum shift can be provided with one of three optional methods:

a) induction acceleration (Section 6.1);
b) electron cooling with an electron beam, which has electron velocity gradient across the beam in the horizontal plane: “velocity gradient electron beam”(Section 6.2);
c) stochastic cooling (Section 6.3).

The storage rate is determined by injection rate at low ion intensity of $1 \div 25$ p/s. In all three cases the storage rate is limited by efficiency of a cooling system, when the ion flux intensity from fragment separator is of $25 \div 10^6$ p/s. Correspondingly, we consider below Three Scenarios. Each of them requires the “individual injection”. The *first Scenario* includes induction acceleration and conventional electron cooling. The *second* one is based on electron cooling with the “velocity gradient electron beam”, in the *third* one a fast stochastic cooling is applied. Both of the last two Scenarios do not need induction acceleration.

All these scenarios can provide the required stacking time value and final choice of the ring design will be determined by technical reasons. Second scenario looks more attractive because of simplest operation of the ring. However its realisation requires experimental investigation of the cooling system with ribbon electron beam and gradient of electron velocity.

The consideration described below shows that the proposed scheme can provide the storage rate of up to $5 \cdot 10^2$ ions/sec.

3. Transfer channel

3.1. The channel scheme

The transfer channel consists of a few different sections (Fig 3.1). An “analyser spectrometer” (position 1) measures individual parameters of every particle delivered by a fragment separator (Table 1.1). The amplified signals from the analyser arrive, with a necessary delay, at two pairs of kickers (positions 2 and 3) for each direction, *x*- and *y*-, which are used for reduction of beam emittance and individual correction of particle trajectories. The profile degrader (position 4) is placed inside achromatic bending section in the region with non-zero dispersion. After crossing the degrader momentum spread of the particles decreases, but due to coupling of longitudinal and horizontal motion the particle trajectory is distorted in the horizontal plane. The distortion is compensated with the second pair of kickers (positions 5 and 6). Required transformations of the particle co-ordinates and angles between different elements correcting the emittance and momentum spread are provided with transfer lines (positions 7) consisting of quadrupole lenses and bending magnets.

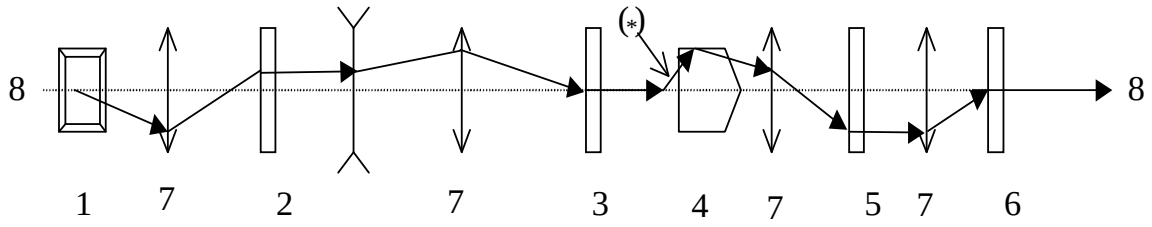

Fig. 3.1. Scheme of the transfer channel,
1- analyser, 2,3- the first pair of the kickers, 4-degrader, 5,6 – the second pair of the kickers, 7 – quadrupole lenses, 8-ion trajectory, (*)-the trajectory of particle with $\Delta p \neq 0$ in degrader region, where $D \neq 0$.

After passing through the first pair of kickers the emittance of the ion beam can be reduced by two orders of magnitude (see Section 3.2). The reduction of ion momentum spread is provided with profile energy degrader (Fig.3.1, position 4), which is located in region with a dispersion *D*(z). The particle momentum spread reduces by 10 times after degrader passing (see Section 3.3). It allows us to reduce significantly the size of an induction betatron core placed in the storage ring and the longitudinal ring acceptance (see Section 5.2). Bending dipole magnets are placed near degrader to form the dispersion of $D \cong 0.5\ m$ in this region.

However non-zero dispersion in the degrader leads to the excitation of the addition betatron oscillations of the ion in the transfer channel when the ion decreases by the value of Δp. The oscillation amplitude equal to $\Delta x \sim D \cdot \Delta p/p$ is comparable with initial values of the angle and displacement. The knowing of individual ion momentum permits to determine individual transverse co-ordinates of every particle after degrader passing. The next kicker pair placed after degrader is necessary to compensate the degrader effect and provide an individual correction of the ion trajectory.

The application of two kicker pairs and the profile energy degrader permits to reduce value of the phase space of an ion-beam by four orders of magnitude with application of the “individual correction” of particle trajectories.

3.2. First kicker system

The kicker system used for the individual correction gets the control signals from the detector of the analyser system. The signals are amplified linearly and transformed to the output amplifier of the kicker power supply. Two kickers are required for individual compensation of horizontal angle and co-ordinate and additional two kickers – for vertical ones. (In principle, the same kicker can provide the kicks in vertical and horizontal directions simultaneously, however it requires more complicated design.) Also additional two pairs of kickers (position 5 and 6 in Fig. 3.1) are required for compensation of emittance increase after degrader section. We consider below the compensation of the horizontal co-ordinate and angle only. The compensation of vertical components is to be provided with two additional pairs of kickers by the same way.

Let's consider the action of two orbit correctors (kickers), which generate the kicks of particle angular deviation of φ_1, and φ_2 to compensate individual horizontal angle and co-ordinate. The principle of the particle trajectory correction with the pair of kickers can be illustrated with the following sketch (Fig 3.2) in the phase space of linear (x) and angular (x') particle co-ordinates. The particle trajectory is shown in Fig. 3.1.

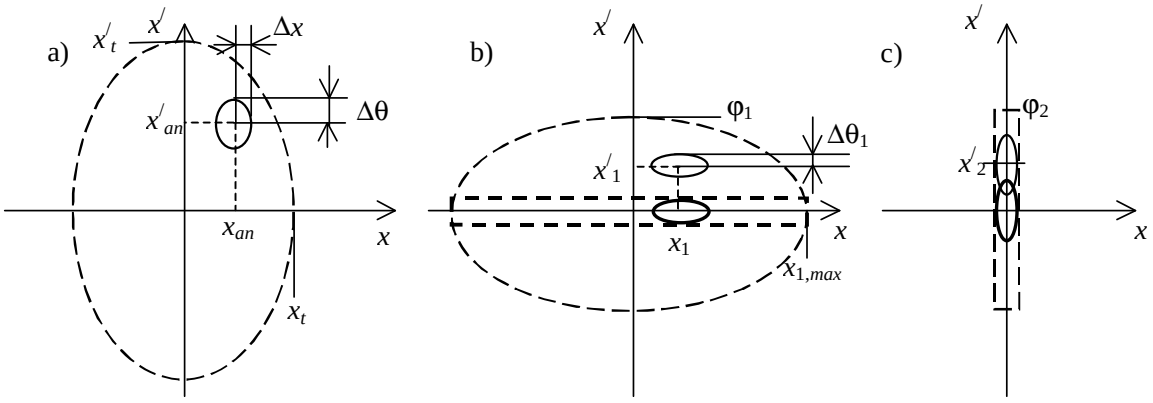

Fig. 3.2. Correction of the particle trajectory using pair of kickers: particle position in (x, x') phase plane (see description in the text) a) initial position (at the analyser exit), b) at the first kicker, c) at the second kicker.

The particle after fragment separator has a co-ordinates x_{an} and x'_{an} measured by analyser with the accuracy of Δx and $\Delta\theta$. It is located in the phase space inside the region at dimensions x_t, x'_t ($x_t \approx 3.5$ mm, $x'_t \approx 50$ mrad, Table 1.1) determined by the primary beam parameters at the target position (Fig. 3.2 a). The transfer line from the analyser to the first kicker transforms the dimensions of the region of the particle location to $x_{1,max}$ and φ_1 – maximum angular deviation of the particle trajectory, which can be corrected with the first kicker. The maximum possible particle co-ordinate inside the kicker:

$$x_{1,\max} = \frac{x'_t x_t}{\varphi_1} \tag{3.1}$$

determines the required kicker aperture.

At the same time the particle co-ordinates are transformed to x_1 and x'_1. The voltage applied to the first kicker provides deflection of the particle trajectory exactly by the angle x'_1. Thereafter the particle is located inside the region at dimensions $x_{1,max}$ and $\Delta\theta_1$ (Fig 3.2 b). The transfer line from the first to the second kicker transforms this region in accordance with maximum possible angular deflection of the particle trajectory with the second kicker φ_2. The second kicker provides deflection of the particle trajectory by the angle x'_2.

Finally, at the exit of the second kicker the particle is located near the axis of the transport channel. It can be easily shown, that in the linear approximation the phase volume of the beam is determined only by the resolution of the analyser and it is equal to $\pi \cdot \Delta x \cdot \Delta\theta$. One has to underline that the beam transformation described here has non-Liouvellion character.

The kicker angle φ is determined by the kicker length l, electric field value E and particle momentum:

$$\varphi = \frac{ZeEl}{Am_p c^2 \beta^2 \gamma}, \tag{3.2}$$

where $m_p c^2$ = 938 MeV, β, γ are relativistic parameters.

One should mention that the voltage at the first kicker is determined by the beam emittance after fragment separator:

$$U \approx E 2x_{1,\max} = K\varphi x_{1,\max} = K x_t x'_t, \; K = 2\frac{A}{Z}\frac{m_p c^2 \beta^2 \gamma}{el} \tag{3.3}$$

and at parameters of Table 1.1 and kicker length of 2 m this value is equal to about 600 kV. In this case, at the ordinary technical field value E = 40 kV/cm the kicker angle (formula 3.2) is about 2.5 mrad and the beam radius in the first kicker is about 7 cm. The voltage at the second kicker and the kicker aperture is substantially less due to reduction of the beam emittance after the first kicker by the value $\Delta\theta/x'_t$.

The first kicker operation at high repetition frequency is main technical problem of the proposed scheme. In principle, the maximum kicker voltage can be reduced by use of a few kickers or by special kicker design (see Section 3.3). All the possibilities will be investigated in details at the stage of the transfer channel technical design. Here for preliminary estimations we assume that the technically achievable repetition frequency is limited by the value of 10 kHz.

A kicker of a finite length introduces certain additional ion displacement

$$\delta x = \varphi \frac{l}{2}. \tag{3.4}$$

Therefore, at optimisation of the channel parameters minimum deflection angle is preferable.

3.3. Limitation of the repetition rate. "Intellectual kicker"

The upper limit of the storage rate in the proposed scheme is related to the first kicker parameters in the transfer channel. It is evident that a kicker operating at voltage of $V \sim 500$ kV and pulse duration of $\tau_{kick} \sim 30$ ns is a very complicated technical installation. In addition the high voltage pulsed generator had to form rectangular pulses of a random distribution in time at a high repetition frequency.

One can simplify the task using special design of the kicker which is applicable in our case (Fig. 3.3 a). The kicker consists of several parallel plates connected with the generator in parallel, therefore the electric field has opposite direction in the neighbor "Subkickers". The generator pulse amplitude changes from pulse to pulse in accordance with the command of the control system ("analyser", which measures a passing ion parameters). To avoid a change of the voltage sign (that simplifies the technique) one can use two kickers, which operate one at a time depending on the ion angular co-ordinate x'. We show in Fig.3.3 a) the ion trajectory when $x' < 0$ and, thereupon the kicker A is turned ON and kicker B is OFF. Correspondingly, the (x, x') phase space is splitted in several parts when kicker A or B has to operate (Fig. 3.3 b).

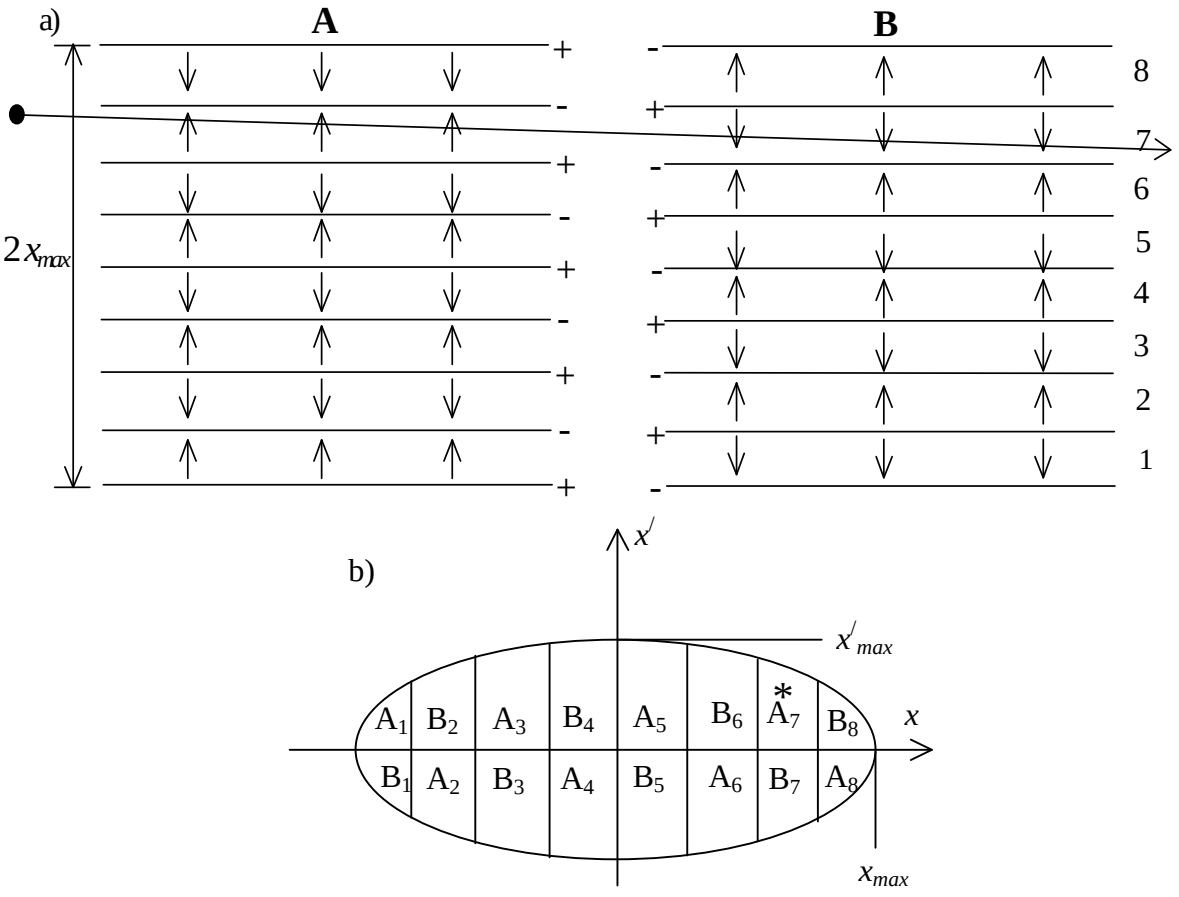

Fig 3.3. The scheme of the multiplate kicker: a) the kicker scheme, b) the ion beam phase space divided in the parts corresponding to the plate number. -> and * - an ion trajectory and position in the phase space.

An important advantage of the proposed scheme is a significant decrease of the kicker voltage amplitude:

$$V_N = \frac{V_0}{N} \ , \tag{3.5}$$

where N is number of the “Subkickers”. The ion loss due to presence of additional plates (which can be made of very thin metallic sheets) is negligible.

We consider another schemes of the kicker, which will be discussed in the next papers. The technical realization of the of the first kicker requires more detail elaboration. Summarizing this consideration one can admit that at realizable kicker parameters its operation repetition rate of

$$f_{rep} \le f_{rep}^{\max} \approx 10^4 s^{-1} \tag{3.6}$$

is achievable. This number will be used below for numerical estimates.

3.4. Transfer lines

The linear transformation maps of the transfer lines from the analyser to the first kicker and between the first and the second kickers can be calculated using standard matrix formalism. Twiss parameters (α, β, γ) of the beam phase area at the target position are related with the emittance:

$$\varepsilon = \gamma_t x_t^2 + 2\alpha_t x_t x_t^{/} + \beta_t x_t^{/2}, \tag{3.7}$$

and $\beta\gamma - \alpha^2 = 1$. In our case at the target position (Fig. 3.2 a) $\alpha_t = 0$, $\gamma_t = 1/\beta_t$, emittance is equal $\varepsilon = \pi \cdot x_t \cdot x_t^{/}$ and betatron function

$$\beta_t = \frac{x_t}{x_t^{/}} \tag{3.8}$$

At the first kicker position we have also $\alpha_1 = 0$. The betatron function is equal:

$$\beta_1 = \frac{x_t x_t^{/}}{\varphi_1^2}. \tag{3.9}$$

Coefficients of the matrix $\boldsymbol{A}$ from the analyser to the first kicker

$$A = \begin{pmatrix} a_{11} & a_{12} \\ a_{21} & a_{22} \end{pmatrix}, \tag{3.10}$$

which provides the transformation of the particle co-ordinate and angle in accordance with

$$\begin{pmatrix} x \\ x^{/} \end{pmatrix}_1 = A \begin{pmatrix} x \\ x^{/} \end{pmatrix}_{an}, \tag{3.11}$$

can be found from the initial and final Twiss parameters using the following relation:

$$\begin{pmatrix}\beta\\ \alpha\\ \gamma\end{pmatrix}_1 = \begin{pmatrix} a_{11}^2 & -2a_{11}a_{12} & a_{12}^2 \\ -a_{11}a_{21} & (a_{11}a_{22}+a_{12}a_{21}) & -a_{22}a_{12} \\ a_{21}^2 & -2a_{22}a_{21} & a_{22}^2 \end{pmatrix} \begin{pmatrix}\beta\\ \alpha\\ \gamma\end{pmatrix}_t . \tag{3.12}$$

When the initial and final values of α function are zero it gives us the following system of equations:

$$\begin{cases} \beta_1 = a_{11}^2\beta_t + a_{12}^2/\beta_t \\ -a_{11}a_{21}\beta_t - a_{12}a_{22}/\beta_t = 0 \\ 1/\beta_1 = a_{21}^2\beta_t + a_{22}^2/\beta_t \end{cases} \tag{3.13}$$

For instance, this transformation can be performed with drift section and thin focusing lens. In this case $a_{11} = 1$ and system (3.13) can be easily solved. The other matrix coefficients written using the beam parameters at the target and the maximum kicker angle have the following values:

$$\begin{aligned} a_{12} &= \frac{x_t}{\varphi_1}\sqrt{1-\frac{\varphi_1^2}{x_t'^2}}, \\ a_{21} &= -\frac{1}{x_t}\sqrt{1-\frac{\varphi_1^2}{x_t'^2}}, \\ a_{22} &= \frac{\varphi_1^2}{x_t'^2}. \end{aligned} \tag{3.14}$$

The required angular deflection of the particle trajectory inside the kicker can be calculated using initial particle parameters measured by analyser:

$$x_1' = -\frac{x_{an}}{x_t}\sqrt{1-\frac{\varphi_1^2}{x_t'^2}} + \frac{x_{an}'\varphi_1^2}{x_t'^2}. \tag{3.15}$$

In the real case, the required transformation of the phase area has to be provided independently in both planes – horizontal and vertical. Therefore transfer line has to include many focusing elements and calculations of its parameters can be performed using special computer codes, for instance MAD. But even in the general case the transformation matrices in both planes will have the same form. For instance, in the horizontal plane the transformation matrix can be expressed using Twiss parameters as follows:

$$\begin{pmatrix} x \\ x' \end{pmatrix}_1 = \begin{pmatrix} \sqrt{\beta_1/\beta_t}(\cos\mu_{01} + \alpha_t \sin\mu_{01}) & \sqrt{\beta_t\beta_1}\sin\mu_{01} \\ -\dfrac{(\alpha_t-\alpha_1)\cos\mu_{01} - (1+\alpha_t\alpha_1)\sin\mu_{01}}{\sqrt{\beta_t\beta_1}} & \sqrt{\beta_t/\beta_1}(\cos\mu_{01} - \alpha_1\sin\mu_{01}) \end{pmatrix} \begin{pmatrix} x \\ x^1 \end{pmatrix}_{an}, \tag{3.16}$$

where the phase advance from the target to the kicker position is calculated as:

$$\mu_{01} = \int_0^{z_1} \frac{dz}{\beta_{x,y}(z)}. \tag{3.17}$$

If in the points "*t*" and "1" alpha function values are equal to zero ($(d\beta/dz)_t = (d\beta/dz)_1 = 0$) the matrix coefficients have a simple form:

$$\begin{pmatrix} \sqrt{\beta_1/\beta_t}\cos\mu_{01} & \sqrt{\beta_t\beta_1}\sin\mu_{01} \\ -\dfrac{\sin\mu_{01}}{\sqrt{\beta_t\beta_1}} & \sqrt{\beta_t/\beta_1}\cos\mu_{01} \end{pmatrix} \tag{3.18}$$

and solution (3.14) corresponds to the case, when $\cos\mu_{01} = \sqrt{\dfrac{\beta_t}{\beta_1}}$. Due to axial symmetry of the problem the matrices in horizontal and vertical plane will differ only by the value of the phase advance.

Thus the signals from the analyser corresponding to the particle spatial angular co-ordinates and position are mixed with coefficients determined by the beam parameters at the target position and the maximum kicker angle and after amplification are applied to the kicker plates. It can be performed, for instance, using fast analogous electronics. The transfer line length and geometry provides a required time delay.

3.5. Degrader section

The profile energy degrader (Table 3.2, Fig. 3.4) is applied to compensate the momentum spread of the ion beam.

Table 3.2. The degrader section parameters.

β_x, β_y - functions, cm	75
Dispersion, D, m	0.5
Degrader thickness, g/cm^2	0.2

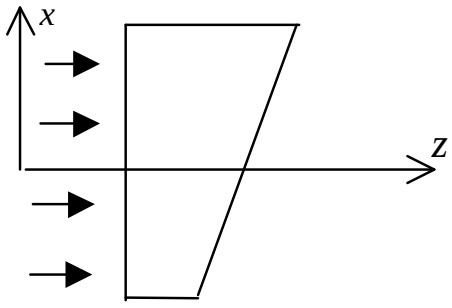

Fig. 3.4. Profile energy degrader

The momentum spread compensation with degrader depends on several effects: amplitude of betatron oscillations, dispersion in degrader section, multiple scattering and energy straggling.

We consider a profile degrader with the thickness linearly increasing with transverse co-ordinate (Fig. 3.4).

When particle passes through degrader the energy shift is determined by ionisation losses dE/dz

$$\Delta E(\Delta p) = \frac{dE}{dz}\Delta z(x), \quad x = D\cdot\Delta p, \tag{3.19}$$

where $\Delta z(x)$ is the dependence of the degrader thickness on transverse co-ordinate, which in its turn depends on ion momentum shift Δp. The ion random betatron phase in degrader produces a variation of transverse co-ordinate of particle and therefore a variation of passage length inside degrader. The ratio of energy variation $\delta\varepsilon$ caused by betatron oscillation to energy shift ΔE is determined by a ratio

$$\frac{\delta\varepsilon}{\Delta E} = \frac{2a}{D\cdot\Delta p/p}, \tag{3.20}$$

where $\Delta p/p = \pm$ 2.5 % is momentum spread before degrader, D is the lattice dispersion at the degrader place.

The energy and momentum spread after profile degrader are equal to

$$\frac{\delta\varepsilon}{E} = \pm\beta^2\frac{2a}{D} \text{ and } \frac{\delta p}{p} = \pm\frac{2a}{D} \approx \pm 2.5\cdot 10^{-3}, \tag{3.21}$$

where D = 0.5 m is the dispersion in the degrader, $a = \sqrt{\varepsilon_{com}\beta_d}$ =0.6 mm is betatron oscillation in degrader, $\varepsilon_{com} \cong 0.5\ \pi\cdot mm\cdot mrad$ is ion beam emittance after kicker compensation, β_d = 75 cm is the beta function in the degrader.

As mentioned above (Section 3.1) the non-zero dispersion at the degrader position excites the ion betatron oscillation when ion decreases its momentum passing the degrader. The betatron amplitude is of the order of

$$\Delta x = D\frac{\Delta p}{p}. \tag{3.22}$$

The increase of beam emittance after degrader corresponds to

$$\Delta\varepsilon_{\text{deg}} = \frac{\Delta x^2}{\beta} = 4\varepsilon_{com}\left(\frac{\Delta E}{\delta\varepsilon}\right)^2 \approx 200\ \pi\cdot \text{mm}\cdot \text{mrad}. \tag{3.23}$$

The 10 times reduction of energy (momentum) spread in degrader gives 400 times increase of beam emittance after degrader. The transverse ion co-ordinate and angle after degrader are equal to

$$x(\Delta p) \approx 12.5 \text{ mm},$$
$$\theta\,(\Delta p) \approx 15 \text{ mrad}. \qquad (3.24)$$

These transverse co-ordinate and angle can be compensated again by second kicker system individually for each particle installed after degrader (position 5 and 6 in Fig. 3.1). The transverse co-ordinate and angle after degrader can be simulated when we know an individual momentum for each particle in analyser.

The thickness of profile degrader in its central part is determined by ionisation losses

$$\frac{dE}{dz} = 0.3\frac{MeV \cdot cm^2}{g}\frac{Z_t}{A_t}\rho_t \frac{Z_{pr}{}^2}{\beta^2}\ln\left(\frac{2\gamma^2\beta^2 mc^2}{I}\right) \approx 6\cdot 10^3 \text{ MeV}\cdot\text{cm}^2/\text{g}, \qquad (3.25)$$

where Z_t, A_t - charge and atomic numbers of the degrader material, ρ_t - degrader density, Z_{pr} - charge number of radioactive ions, $\beta = v/c$, v – ion velocity, c – light spead, $I = 13{,}5\cdot Z_t$ (eV) - ionisation potential of degrader atoms. For light degrader with $Z_t = 6$ and $\rho_t = 1.1$ g/cm^3 the maximum thickness of the profile energy degrader corresponds to

$$\Delta z_{\text{deg}} = 1{,}9 \text{ mm}. \qquad (3.26)$$

The multiple scattering in degrader produces an additional ion angular spread of

$$\bar{\theta}^2 = 0{,}25\frac{Z_t(Z_t+1)}{A_t}\frac{Z_{pr^2}}{E^2}t = 0.1\ mrad^2,\ \sqrt{\bar{\theta}^2} = 0.3\ mrad, \qquad (3.27)$$

where $\sqrt{\bar{\theta}^2}$ is angular spread in mrad in (3.24), t is degrader thickness in $\mu g/cm^2$ and E is ion energy in MeV. The multiple scattering angle in degrader together with betatron oscillations determine a resolution angle after degrader

$$\delta\theta_{res} \approx \left(\frac{\varepsilon_{com}}{\beta_d} + \bar{\theta}^2\right)^{1/2} \approx 0.9\ mrad. \qquad (3.28)$$

The fluctuation of energy losses - energy straggling produces an additional energy spread after degrader. The ionisation losses are statistical in nature. The probability distribution function is equal to [5]:

$$f(z,\Delta\varepsilon) = \frac{1}{\sqrt{2\pi\gamma z}}e^{-\frac{(\Delta\varepsilon-\alpha z)}{2\gamma z}}, \qquad (3.29)$$

where $\Delta\varepsilon$ is mean energy losses,

$$\gamma z = \xi E_{\max}\left(1-\frac{1}{2}\beta^2\right),$$

$$\xi = \frac{2\pi n e^4 Z_{pr}^2}{m_e v_{pr}^2} Z \cdot t \approx 100 \cdot mc^2,$$

$$E_{\max} = \frac{2m_e \beta_{pr}^2 \gamma_{pr}^2 c^2}{1 + 2\gamma_{pr}\left(\frac{m_e}{m_{pr}}\right) + \left(\frac{m_e}{m_{pr}}\right)^2} \approx 2MeV, \tag{3.30}$$

where $E_{\max}$ is the maximum energy transferable by a fast moving charged particle to the electron, n is the number of target atoms per unit volume, Z_{pr} the ion charge, t is target thickness, m_e is electron mass. The fluctuation of ionisation losses is equal to

$$\delta\varepsilon_{ion} = \sqrt{\xi E_{\max}\left(1 - \frac{1}{2}\beta^2\right)} = 10 \ MeV. \tag{3.31}$$

The energy spread related to energy straggling corresponds to

$$\frac{\delta\varepsilon}{E} = \frac{\delta\varepsilon_{ion}}{AE} = 1.5 \cdot 10^{-4}. \tag{3.32}$$

The input of energy straggling is essentially less than energy spread related to betatron oscillations and it is compared with energy resolution in analyser.

The horizontal co-ordinate resolution after degrader is equal to

$$\delta x_{res} = 2\sqrt{\varepsilon\beta_d} + D \cdot \sqrt{(\Delta p / p)^2 + (\delta\varepsilon_{ion} / \beta^2 AE)^2} \approx 1.3 \text{ mm}. \tag{3.33}$$

The resolution of momentum after degrader corresponds to

$$\delta p / p_{res} \approx \pm 5 \cdot 10^{-4}. \tag{3.34}$$

3.6. Second kicker system

The second kicker system (position 5 and 6 in Fig. 3.1) is used for an individual compensation of transverse ion angular and spatial co-ordinates after degrader passing. These transverse co-ordinates are determined by individual particle momentum. The individual anglular and co-ordinate resolution in analyser $\delta\theta$ and δx in the kicker system is transformed into the angular resolution

$$\Delta\theta = \frac{\delta x_{res}}{2\sqrt{\beta_d \beta_2}} + \frac{\delta\theta_{res}}{2}\sqrt{\frac{\beta_d}{\beta_2}} \cong 1.6 \cdot 10^{-4} \text{ rad}, \tag{3.35}$$

where $\beta_d = 7.5$ cm and $\beta_2 = 40$ m –are beta functions in the degrader and the second kicker. The resolution restriction in the analyzer produces an ion co-ordinate uncertainty after the second kicker of

$$\Delta x = \sqrt{\varepsilon\beta_2}\,\frac{a_k}{2\beta_2} + \frac{\delta x_{res}}{2}\sqrt{\frac{\beta_2}{\beta_d}} + \frac{\delta\theta_{res}}{2}\sqrt{\beta_d \beta_2} \cong 9 \text{ mm}. \tag{3.36}$$

The beam emittance after the degrader and kicker compensation is equal to

$$\varepsilon_{com} \cong \Delta x \Delta\theta \cong 1.5\ \pi \cdot mm \cdot mrad\ . \tag{3.37}$$

The beam emittance after kicker compensation by 10 times higher than "individual emittance of particle" of $\varepsilon_{ind} \approx 0{,}2\pi \cdot mm \cdot mrad$ and two order less than beam emittance before compensation. The momentum spread after profile degrader is equal to

$$\frac{\delta p}{p} \approx \pm 2.5 \cdot 10^{-3}. \tag{3.38}$$

4. Scheme of the storage ring. Three operation scenarios

In *the first scenario* we propose the strong focusing storage ring (Fig. 4.1) containing injection system - septum and kicker, induction acceleration station ("inductor"), electron cooling system and RF system.

An injected ion with momentum shift $\Delta p < 0$ relatively to average momentum of the stacked ions ("the stack momentum") endures immediately after injection accelerating action of the induction electric field and electron cooling force simultaneously. After certain time the ion comes to the stack. Due to evident technical reasons the stack orbit (the equilibrium orbit) penetrates induction core as well. Therefore, several conditions have to be met:

1) the electron cooling has to be capable to keep the stack ions at a constant momentum (or to prevent further deceleration action of inductor at small momentum difference for an injected ions and a stack ions);

2) induction acceleration has to be sufficiently fast for injected ions with a large initial momentum shift than the acceleration due to electron cooling;

3) the kicker operation applied for new injected ion has not to disturb the motion of the previous injected ions when they travel to the stack and the stack ions as well.

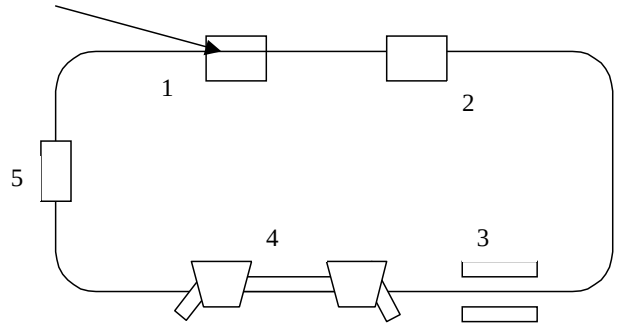

Fig.4.1. Scheme of the storage ring for individual injection and cooling.
1- septum, 2-kicker, 3- induction deceleration station, 4-electron cooler, 5-RF station.

The second operation scenario assumes application of the modified electron cooler with transverse (horizontal) gradient of longitudinal electron velocity that provides fast cooling both injected ions with large momentum shift and stack ones. The inductor is not used in the second scenario.

The third scenario assumes application of a fast stochastic cooling. The betatron inductor and electron cooler are not used in this scenario.

The estimates show that one can reach with the first and second scenarios the ion storage rate up to $5 \cdot 10^2$ ions/sec if the conditions $1 \div 3$ are met and a special kind of kicker pulse synchronisation is applied – "the individual injection", as we call such a regime.

5. Individual injection in the storage ring

5.1. Injection kicker operation

The main problem for designing the injection scheme is in our case a random character of radioactive ion generation. They arrive at the ring septum one by one separated in time by the interval

$$\Delta t_{inj} = \tau_{inj}(1 \pm \delta),\ \tau_{inj} = \frac{1}{\hat{N}_i}, \tag{5.1}$$

where $\hat{N}_i$ is the average value of ion flux. Δt_{inj} is a random value, which has a is root mean square value $\delta \approx 1$ of the interval fluctuation. In the injection scheme proposed here we assume that *the stored stack is bunched* at the first harmonic of the ion revolution frequency in the ring.

The injection kicker operating in the pulsed mode with the pulse duration much shorter of the ion revolution period T_{rev} brings a new injected particle directly info the stack orbit (Fig. 5.1).

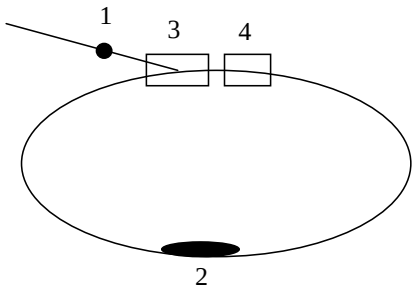

Fig. 5.1. Injection scheme in the ring. 1 - injected particle in the transfer channel, 2 - stack in equilibrium orbit, 3 - septum, 4 - kicker.

However, the kicker operation has to be synchronised with the stack (Fig. 5.2): it can not operate when the stack circulating in the ring passes the kicker, either the stack particles are lost. One has to underline that the dispersion in the kicker section is equal to zero to avoid exitation of betatron oscillations of an injected ion. Thus, the kicker has to be synchronised with the signals from the "analyser" and with the ring RF system (Fig. 5.2). It should be noted, that in all three scenarios *the RF system is ON* during the ion injection cycle, and the kicker operation is synchronised with the bunch (stack) revolution independently of the ion flux intensity.

The synchronisation of the kicker operation with the bunch revolution leads to decrease of the injection efficiency

$$\eta_{inj} \le 1 - \frac{l_b}{C}, \tag{5.2}$$

however at the bunch length of $l_b \approx 3$ m, and ring circumference $C = 250$ m the value of η_{inj} is, practically, equal to unit.

The individual injection scheme is somewhat different for different intensities of the injected ion fluxes. One can distinguish two outmost cases:

$$\hat{N}_i < \tau_{st}^{-1} \text{ - low intensity ion flux,} \tag{5.3}$$

$$\hat{N}_i > \tau_{st}^{-1} \text{ - high intensity ion flux,} \tag{5.4}$$

where τ_{st} is the stacking time.

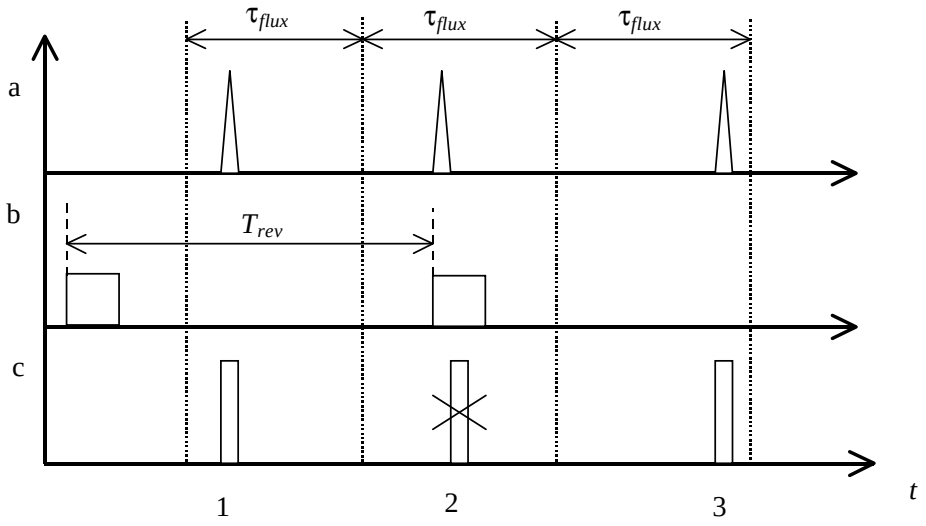

Fig. 5.2. Kicker synchronisation:
a- trigger signal from the analyser, b- “forbidding” signal from stack (from the ring RF station), c-kicker operation, 1, 3 – kicker pulse is permitted, 2 - kicker pulse is forbidden.

In the second operation scenario the ring can be operated in the continuos mode, when the ion injection takes a place during stacking process. The firs and third scenarios presume the periodic mode of the injection operation: the stacking procedure can be performed after injection cycle completion only. In this case the injection of new ions during the stacking is impossible. It is related to peculiarities of the induction accelerator operation in the first scenario, and to requirements of the stochastic cooling system in the third one.

5.2. Second operation scenario. Storage rate at continuous injection

Initially we consider the case with a continuos injection. Here, the ion after injection moves into the stack during the τ_{st} time. When the ion flux intensity is low (the condition 5.3) new injections do not occur during the stacking process and storage rate is merely equal to the ion flux:

$$R_{store} = \hat{N}_i . \tag{5.5}$$

As it will be shown in the Section 6 one can achieve the stacking time of 10 – 50 ms, and the storage rate corresponds to R_{store} = 1 – 100 ions/sec.

In the case when the ion flux intensity exceeds this level new injection pulses happen during the stacking of the injected ion. Then during the injection the ion circulating in the ring can be lost if it passes inside the kicker when it pulses (the kicker operation is synchronised with the stack revolution only). The probability of the particle loss after single injection can be estimated as a ratio between the kicker pulse duration and the ion revolution period: τ_{kick}/T_{rev}. The injection pulses number during the stacking is equal to $\hat{N}_i\tau_{st}$. The stacking efficiency can be estimated as an ion survival probability during the stacking:

$$\eta_{st} = \left(1 - \frac{\tau_{kick}}{T_{rev}}\right)^{\hat{N}_i\tau_{st}} . \qquad (5.6)$$

Here we assume that $\tau_{kick}/T_{rev} >> l_b/C$. The storage rate can be estimated then with the following expression:

$$R_{store} = \left(1 - \frac{\tau_{kick}}{T_{rev}}\right)^{\hat{N}_i\tau_{st}} \cdot \hat{N}_i , \qquad (5.7)$$

which includes the expression (5.5) as a limit case. The function $R_{store}(\hat{N}_i)$ has maximum at

$$\hat{N}_i^* \approx \frac{T_{rev}}{\tau_{st}\tau_{kick}} , \ \tau_{kick} << T_{rev} \qquad (5.8)$$

and the maximum value is equal to (Fig. 5.3 and 5.4)

$$R_{\max} = \left(1 - \frac{\tau_{kick}}{T_{rev}}\right)^{T_{rev}/\tau_{st}} \cdot \frac{T_{rev}}{\tau_{st}\tau_{kick}} . \qquad (5.9)$$

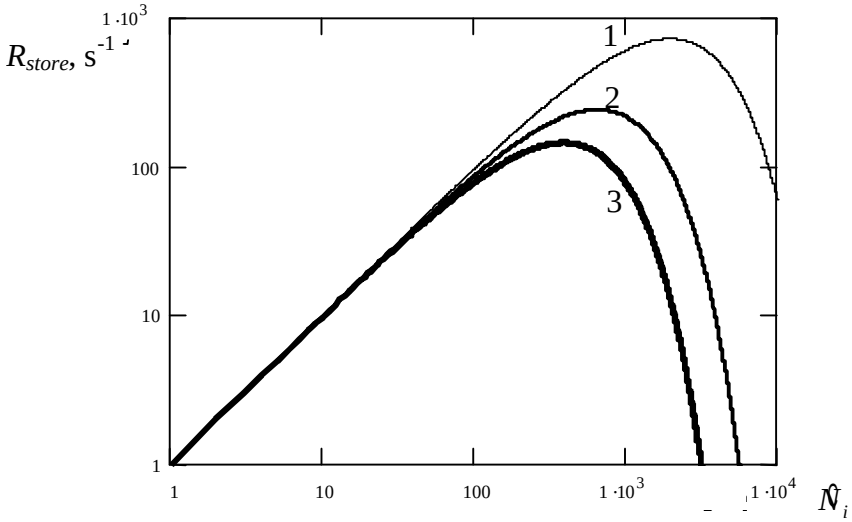

Fig. 5.3. The ion storage rate as the function of the ion flux at continuos injection. The kicker pulse duration is 50 ns, the stacking duration is 10 (curve 1), 30 (curve 2) and 50 (curve 3) ms.

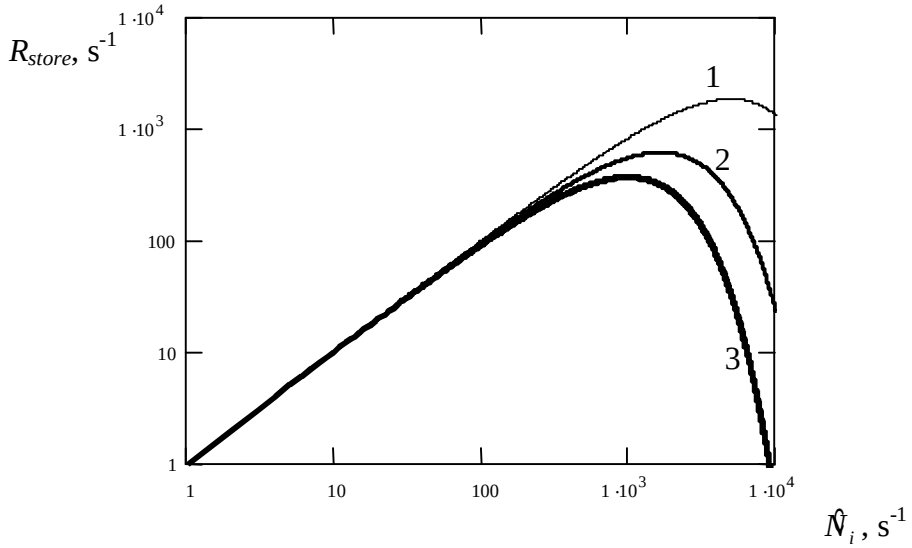

Fig. 5.4. The ion storage rate as the function of the ion flux at continuos injection. The kicker pulse duration is 20 ns, the stacking duration is 10 (curve 1), 30 (curve 2) and 50 (curve 3) ms.

At the discussed injection scheme there is some optimum ion flux corresponding to the maximum storage rate. The value of the optimum flux increases with decrease of τ_{kick}/T_{rev} and with decrease of the stacking duration. At realistic parameters of the injection kicker and stacking process duration (Section 6.2) the optimum ion flux is about a few thousands of ions per second and stacking efficiency can be about 50%. This regime of the ring operation seems to be very attractive, because it can provide the storage rate of about 10^3 ions/sec at repetition frequency of o few kHz. It is very important for operation of the first kicker in the transfer channel to have it repetition as low as possible (see Section 3.2).

5.3. Storage rate at periodical injection

Let's start with *the second scenario*, where the electron cooling works continuously. One can see from the Fig. 5.3 and 5.4 that continuos injection is not effective at the ion flux higher than about 10^3 ions/s. It is caused by the fast decrease of the ion survival probability at high frequency of injection kicker pulses during the stacking process. Seemingly one can avoid this limitation using a periodical injection. In this case the injection is permitted only during a short time interval τ_{inj}, which is less than the stacking duration. After the injection and stacking cycle completion all the injected ions are stacked and the next injection can be performed. The injection cycle duration can be chosen from the maximum of the storage rate. The storage rate can be estimated by the expression similar to (5.7):

$$R_{store} = \frac{\left(1 - \frac{\tau_{kick}}{T_{rev}}\right)^{\hat{N}_i \tau_{inj}} \hat{N}_i \tau_{inj}}{\tau_{stack}} \qquad (5.10)$$

However, at the second operation scenario the periodical injection does not lead to increase of the storage rate (Fig. 5.5). At increase of the ion flux the optimum injection duration decreases and maximum storage rate keeps the same value. Thus, at high ion flux intensity the

continuous injection is optimal, if the stacking process is performed using an electron cooling system with a gradient of the electron longitudinal velocity. The optimum repetition frequency of the kickers operation in this case is determined by the ratio τ_{kick}/T_{rev} and by the stacking process duration.

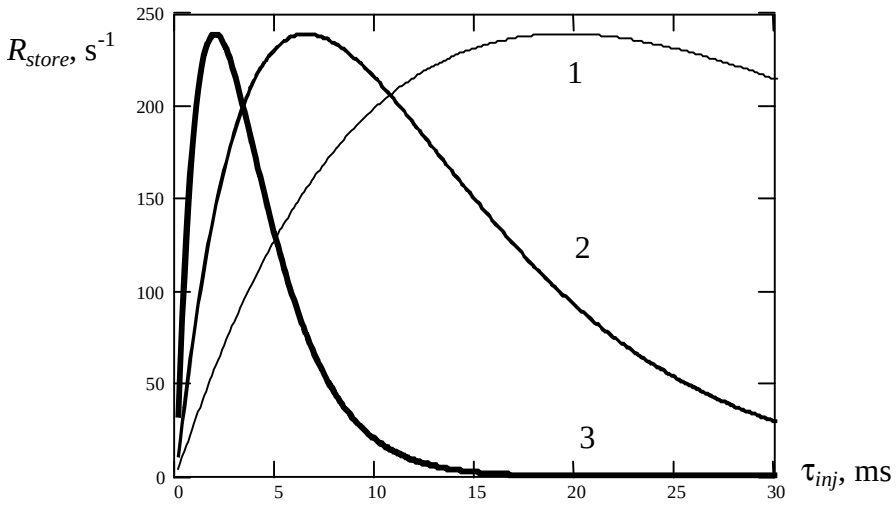

Fig. 5.5. The ion storage rate dependence on the injection period duration. Periodical injection, second operation scenario, τ_{kick}/T_{rev} = 0.05, τ_{st} = 30 ms, ion flux is 10^3 (curve 1), $3\cdot10^3$ (curve 2) and 10^4 (curve 3) ions/s.

At the first and third operation scenarios only the periodical injection can be used, and storage rate in both these cases can be estimated as follows:

$$R_{store} = \frac{\left(1-\frac{\tau_{kick}}{T_{rev}}\right)^{\hat{N}_i\tau_{inj}} \hat{N}_i\tau_{inj}}{\tau_{inj}+\tau_{stack}}. \qquad (5.11)$$

The difference between this expression and expression (5.10) reflects the fact that at the first and third scenarios the stacking is impossible during the injection.

Fig. 5.6 shows that at the same kicker pulse duration and stacking time values the efficiency of the first and third scenarios practically coincides with the efficiency of the second scenario only at flux intensity near 10^4 ions/s. At intensity of the ion flux of $10^2 \div 10^3$ ions/s the storage rate at the first and second scenarios with periodical injection is $1.5 \div 2$ times less that at second scenario and continous injection. And at very low ion flux all three scenarios are equivalent – the storage rate is practically equal to the ion flux.

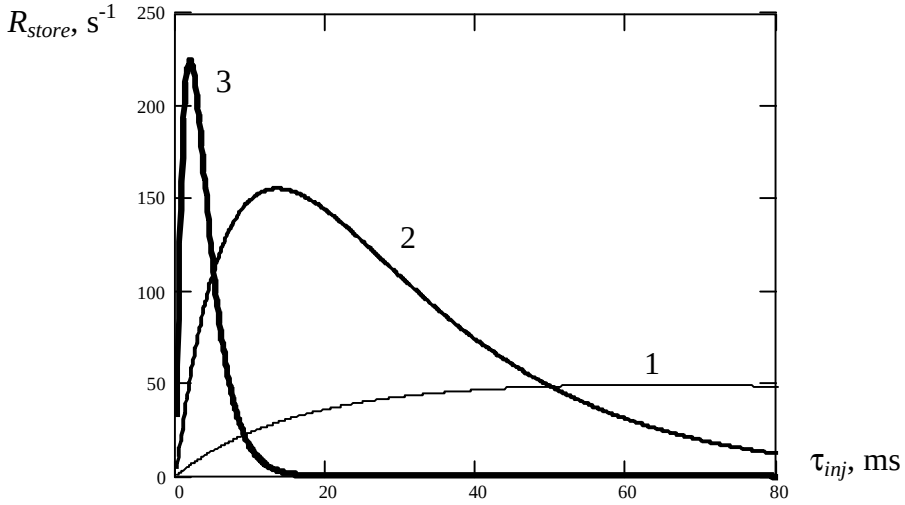

Fig. 5.6. The ion storage rate dependence on the injection period duration. Periodical injection, first and third operation scenario, τ_{kick}/T_{rev} = 0.05, τ_{st} = 30 ms, ion flux is 10^2 (curve 1), $\cdot 10^3$ (curve 2) and 10^4 (curve 3) ions/s.

5.3. Periodical injection at very high intensity of the ion flux

At the ion flux intensity significantly larger than maximum repetition frequency of the first kicker in the transfer channel the injection kicker operation can be synchronised both with the revolution of ions circulating in the ring and with the stack revolution. To provide an effective injection without knocking out a stored ion, one has to know the position of every stored ion in the ring (position 4 in the Fig. 5.7) before it comes to the stack. However the ion revolution frequency of different ions depends on their particular momentum shift Δp:

$$\frac{\Delta\omega}{\omega} = \eta_\omega \frac{\Delta p}{p} \approx 5 \cdot 10^{-3}, \quad \eta_\omega = \frac{1}{\gamma^2} - \frac{1}{\gamma_{tr}^2}, \tag{5.12}$$

where γ_{tr} - Lorenz factor at transition energy.

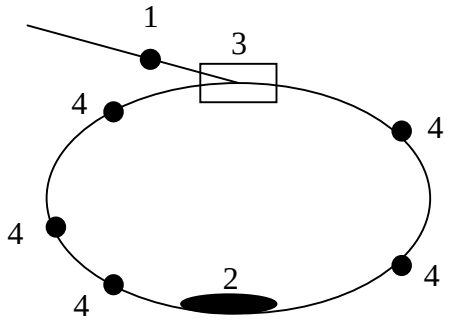

Fig. 5.7. Injection scheme in the ring at a very high intensity flux. 1 - injected particle in the transfer channel, 2 - stack in equilibrium orbit, 3 - kicker, 4 – the stored particles placed outside the stack

Therefore the position of the circulating ions is completely unpredictable after some "mixing" time:

$$\tau_{mix} \sim T_{rev} \frac{\omega}{\Delta\omega}, \tag{5.13}$$

where T_{rev} is the average value of the ion revolution period. If the injection cycle duration is less than the mixing time one can calculate a moment of time when each ion circulating in the ring passes the injection kicker. When the new ion came from the fragment separator the kicker pulse is applied only in the case if inside the injection kicker vicinity there are no ions circulating in the ring.

To estimate a storage rate for this injection scheme let's imagine that the ring circumference is divided into a few equal intervals and the interval number is determined by the ratio between the injection kicker pulse duration and the ion revolution period: T_{rev}/τ_{kick}. The stack occupies one of these intervals and injection of new ion is provided only inside the empty interval. Every circulating ion occupies its own interval (Fig. 5.7) and injection is repeated until all the intervals are occupied. If the ion flux is significantly larger than the kicker repetition frequency f_{rep} this procedure will be completed after the time:

$$\tau_{inj} = \frac{T_{rev}}{\tau_{kick} f_{rep}}, \tag{5.12}$$

and the storage rate can be estimated by the expression:

$$R_{store} = \frac{T_{rev}}{\tau_{kick}} \frac{1}{\tau_{inj} + \tau_{st}}. \tag{5.13}$$

The condition

$$\tau_{inj} << \tau_{mix} \tag{5.14}$$

can be satisfied by corresponding choice of the ring transition energy.

At the parameters of the Fig. 5.6 and the kicker repetition frequency of 10 kHz the storage rate is about $7 \cdot 10^2$ ions/s. This value exceeds the storage rate at the ion flux of 10^4 ions/s by about 3 times.

Thus, at the individual injection of the ions the storage rate increases with an increase of the ion flux intensity and reaches the level of $5 \cdot 10^2 \div 10^3$ ions/s when the flux intensity is equal to the kicker repetition frequency. At the ion flux of 10^4 ions/s the storage rate exceeds that one of the scheme described in the Section 1 by about two orders of magnitude. At the ion flux of 10^6 ions/s and higher the storage rate can be increased by about 3 times at the same repetition frequency of the kicker operation (10 kHz) by synchronisation of the kicker pulses with the ions circulating in the ring. At high ion flux intensity the achievable storage rate is comparable with other storage schemes (see Section 1).

6. Fast stacking in the storage ring

As we have shown above (Section 3) the "individual particle emittance" at the exit of the transfer channel is about $\varepsilon_{in} = 1.5\ \pi \cdot mm \cdot mrad$ and momentum spread is less than $\delta\rho/\rho \approx \pm 2.5 \cdot 10^{-3}$. Therefore the acceptance of the storage ring can be relatively small - of $5 \div 10\ \pi \cdot mm \cdot mrad$ in this case. It is the main advantage of the "individual correction" of the particle trajectory in the transport channel. An application of the "individual particle injection" (described in the previous section) permits to store in the ring 10-20 ions during injection period of duration of about a few ms (depending on the ion flux from fragment separator). The individual injection presumes that the stacked beam is bunched during injection period and injection kicker operation is synchronised with the bunch revolution.

After injection cycle the momentum of every new injected ion is shifted relatively to the "stack momentum" by the value less than about $5 \cdot 10^{-3}$. Such a momentum spread is rather high to produce a fast cooling of the ions using a conventional electron cooling system. We consider below a stacking cycle of duration of about $\tau_{st} \approx 20 \div 30$ ms. To provide the fast stacking of the injected ions we propose three possibilities:

1) to use a conventional electron cooling system working at the stack energy and to compensate the initial momentum deviation of the injected ions using induction acceleration;

2) to use an electron cooling system with an electron beam having a gradient of electron longitudinal velocity across the beam; the cooling system is placed in the position with non-zero dispersion and electron velocity gradient provides effective cooling of the ions independently on their momentum;

3) to use a longitudinal stochastic cooling; in this case after the injection complete the RF system has to be switched off, the ion beam is stochastically cooled down, thereafter the "cooled" coasting beam has to be bunched again;

All these possibilities can provide the required stacking time value and a final choice of the ring design will be determined by technical reasons. The second possibility looks more attractive because of the simplest operation of the ring. However its realisation requires experimental investigation of the cooling system with a ribbon electron beam and gradient of electron velocity.

6.1 First operation scenario: betatron inductor and electron cooler

6.1.1. General description. Working cycle

The main feature of the storage ring scheme described in this section is an application of electron cooling and induction betatron acceleration. This method of accumulation employs the beam emittance and momentum spread (and, as a result, the bunch length) compression through electron cooling that opens the space for new successive cycles of the beam injection. The use of induction betatron acceleration permits to provide fast variation of the ion momentum, when electron cooling is not effective yet due to large initial difference between the ion and electron velocities.

We choose the ring parameters in such a manner that every injected ion has negative momentum shift $\Delta p < 0$ relatively to average momentum of the stacked ions ("the stack momentum"). Immediately after injection the ion endures accelerating action of the induction electric field and electron cooling force simultaneously. Therefore after certain time the ion comes to the stack. The induction deceleration has to be sufficiently fast for injected ions with a large initial momentum shift where electron cooling force is small. Fig. 6.1 shows the force behavior in the electron rest frame.

The electron cooling force strongly depends on the ion momentum shift Δp [5]

$$F \propto \begin{cases} \dfrac{\Delta p}{p}, \dfrac{\Delta p}{p} << \left(\dfrac{\Delta p}{p}\right)_e & \left(v_i << \Delta_{\parallel}\right), \\ \dfrac{1}{\left(\dfrac{\Delta p}{p}\right)^3}, \dfrac{\Delta p}{p} >> \left(\dfrac{\Delta p}{p}\right)_e & \left(v_i >> \Delta_{\parallel}\right) \end{cases}, \tag{6.1}$$

where $(\Delta p/p)_e$ is relative longitudinal momentum spread of electrons in the laboratory reference frame (LRF), V_i and $\Delta_{\parallel}$ are ion velocity and electron velocity spread in the electron rest frame.

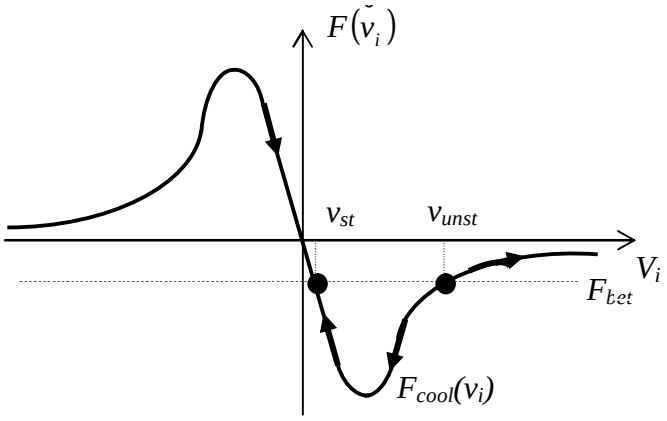

Fig. 6.1. The dependence of cooling friction force (solid curve) and betatron acceleration force (dashed line) on longitudinal ion velocity in electron rest frame.

Actually the cooling friction force is sufficiently high for cooled stack ions, which have momentum spread of $\Delta p/p \cong 10^{-4}$. However, it is rather low for new injected ions with momentum spread of $\Delta p/p \approx 2\delta p/p \cong 5\cdot 10^{-3}$ (see (3.46)) caused by positive momentum shift for every injected ion mentioned above.

To produce a fast acceleration of new injected ions to the stack an induction betatron accelerator can be used. The ions will be cooled and keep in the stack when maximum of the friction force F_{cool} is higher than acceleration betatron force F_{bet} (Fig. 6.1):

$$\left(F_{cool}(v_i)\right)_{\max} > F_{bet}. \tag{6.2}$$

The cycle of the ring operation during in the first scenario (Fig. 6.2) starts with injection of $n \sim 10$ ions during certain injection time, which is determined by the ion flux $\hat{N}_i$. It is less than $\tau_{inj} \approx 5$ ms at a high ion intensity (Fig. 5.6). As assumed above the energy of all injected particles is less than energy of the stack that corresponds to the maximal energy of ions after passing the degrader. Then the ions are decelerated by the inductor during $\tau_{st} \approx 20$ ms to the stack energy. If the same injected ions reach the stack before induction voltage is OFF, they are captured in the stack by electron cooling force, which is stronger of betatron acceleration force. The ions endure simultaneously with electron cooling an action of RF voltage, which is produced by RF station operated at the first harmonics of the ion revolution frequency. Therefore the cooled ions are captured into RF separatrix. At the RF voltage of the order of 300 V the stack bunch size is about 3 m. When acceleration of new n ions is finished the induction voltage changes the sign and stays negative during second half of the period $\Delta t \sim 20$ ms when the betatron core field decreases (Fig. 6.2). Thereafter the injection is repeated again. Thus the injection periodicity in the first operation scenario is about

$$T_{inj} = \tau_{bet} \approx 40 \text{ ms}, \tag{6.3}$$

where $\tau_{bet} \sim \tau_{stack} \sim$ 20 ms is induction acceleration time.

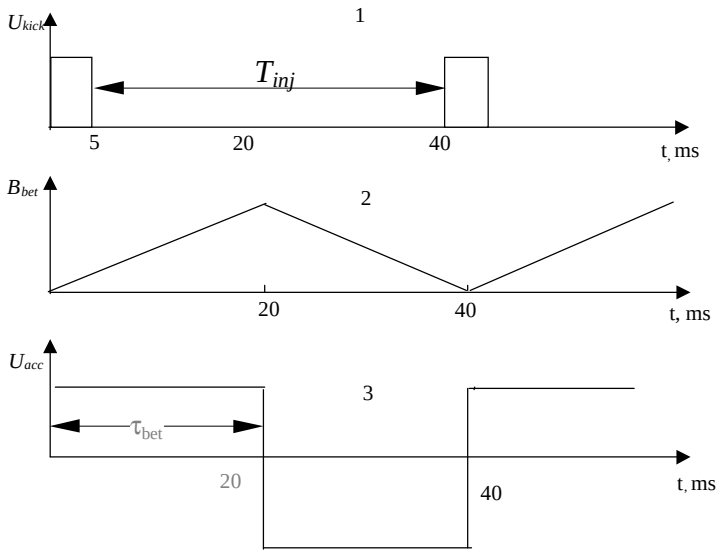

Fig.6.2. The ring operation cycle, 1 – envelope of the kicker pulses, 2- magnetic field in betatron core, 3 - accelerating (decelerating) voltage in betatron induction accelerator.

6.1.2 Betatron induction accelerator

The energy of the stack and injected ions is different. The minimal energy of the injected ions corresponds to the stack ion energy, and their maximum energy is shifted by $2 \cdot \Delta E$:

$$\Delta E = \beta^2 \gamma A m_p c^2 \left(\frac{\Delta p}{p} \right)_{\max}. \tag{6.4}$$

The betatron induction accelerator produces a fast deceleration from individual injection energy to the stack energy. The force F_{ind} produced by the induction accelerator does not depend on individual ion momentum shift and determined by the accelerating voltage $U_{acc} \sim 100\ V$:

$$F_{ind} = \frac{ZeU_{acc}}{C} \approx 40\, {eV}/{cm}, \tag{6.5}$$

where C is the ring circumference. The increase of ion energy per turn corresponds to

$$\Delta E_{turn} = ZeU_{acc} \cong 5\ \text{keV}, \tag{6.6}$$

and the acceleration time τ_{acc} is related to the turn number N_{turn} as follows:

$$\tau_{acc} = N_{turn} T_{rev},\ N_{turn} = \frac{\Delta E}{ZeU_{dec}}, \tag{6.7}$$

where $T_{rev} \approx 1\mu s$ is the ion revolution period, ΔE – the ion energy shift (6.4). Thereupon one can write the following formula for acceleration voltage

$$U_{acc} = \beta^2\gamma \frac{m_p c^2}{e} \frac{Z}{A} \left(\frac{\Delta p}{p} \right)_{\max} \frac{T_{rev}}{\tau_{acc}} \approx 100\ \text{V}, \tag{6.8}$$

where $(\Delta p/p)_{max} = 0.5\%$ (Section 3). This value determines the size of the inductor:

$$B_{\max} S = \int U dt = U_{acc} \tau_{acc} = \beta^2\gamma \frac{m_p c^2}{e} \frac{Z}{A} \left(\frac{\Delta p}{p} \right)_{\max} T_{rev}, \tag{6.9}$$

where S is the inductor core cross section, $B_{max} = 1.5$ T is magnetic field in the iron core. The core (Fig. 6.3) has the shape of a ring with rectangular cross section of the sizes $l = 1.2$ m, $h = 1.4$ m, which fit to the chosen parameter values.

The inductor coil current I can be estimated from the following expression:

$$B = 0.4\pi\mu \cdot \frac{N_{coil} I}{2\pi D}, \tag{6.10}$$

from whence we find $I \approx 250$ A if the turn number in the coil is $N_{coil} = 20$, the average coil diameter is $D = 1$ m and the permeability of the core material is $\mu = 600$. The accelerating voltage is applied to the gap formed in the metallic chamber wall with a ceramic passage insulator (Fig. 6.3., position 4).

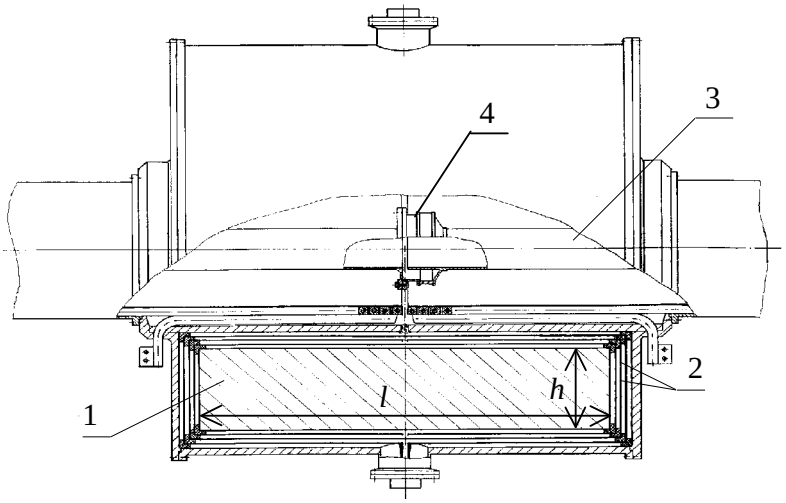

Fig. 6.3. The betatron inductor scketch. 1 – inductor core, 2 – copper screens, 3 – vacuum chamber, 4 – passage insulator (ceramic tube).

6.1.3. Electron cooling

One of the basic elements of the storage ring is electron cooler. Its main peculiarity is a high quality of magnetic field in cooling section, which is necessary to reach the maximum of longitudinal cooling force equal to [6]:

$$F_{\max} = \frac{Z^2 e^2 n_e^{2/3}}{4\pi\varepsilon_0} \cong 75 \;\; eV/cm, \tag{6.11}$$

where $n_e = 10^8$ cm^{-3} is the electron beam density in the electron reference frame at the electron beam current of I = 0.3A and electron beam radius of 0.5 cm, Z = 50 is the ion charge number.

The requirement to the magnetic field homogeneity is very hard: the transverse magnetic field component in the cooling section has to be of the order of

$$\frac{B_\perp}{B_{cool}} \le 3 \cdot 10^{-5}, \tag{6.12}$$

where B_{cool} = 1,5 kG is the magnetic field in the cooling section. The results of many experiments (Fig. 6.4) [7] may differ significantly namely due to different quality of magnetic field in the coolers.

The cooling force dependence on ion velocity near its maximum can be described by the approximation formula [8]

$$F_{cool} = \frac{25\sqrt{5}}{16} \cdot F_{\max} \frac{(2v_F)^4 v_i}{\left[(2v_F)^2 + v_i^2\right]^{5/2}}, \quad v_F = 2c\sqrt{r_e n_e^{1/3}}, \tag{6.13}$$

where $v_F \cong 6 \cdot 10^5$ cm/s is electron velocity spread in the electron reference frame, v_i is the ion (to be cooled) velocity in there, r_e is electron classic radius. To keep the ions in the stack

when the inductor voltage is ON, one needs to provide the cooling force maximum higher than F_{bet} (6.2).

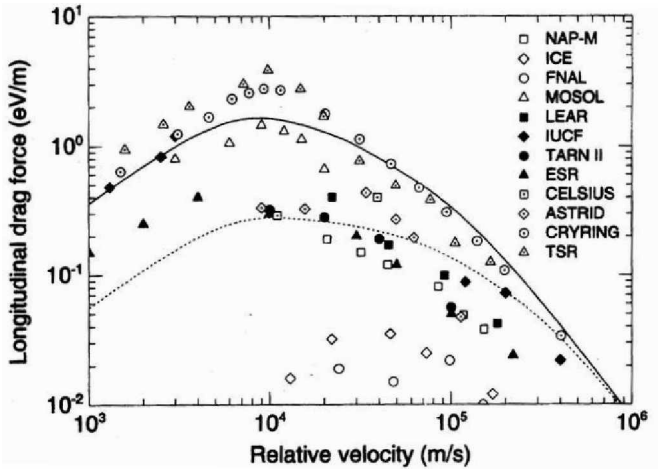

Fig. 6.4. Experimental dependence of longitudinal cooling force on longitudinal ion velocity normalized to single charge ions (F_{max}/Z^2) and electron density of 10^8 cm^{-3} for different storage rings.

Intrabeam scattering restricts the minimal ion velocity spread in the stack. At an enhancement of the stacked ions number N_{st} their equilibrium momentum spread increases as

$$\frac{\Delta p_{st}}{p} \propto N_{st}^{1/2}, \tag{6.14}$$

and is of the order of 10^{-4} for $N_{st} = 10^6$-10^7 at an electron beam density of $n_e = 10^8\,\mathrm{cm}^{-3}$.

An RF system with a small RF voltage of $U_{RF} \approx 1$ kV operated at the first harmonics of the ion revolution frequency is installed in the ring. At electron cooling the ion momentum spread becomes small and ions are captured in the RF separatrix. The stack occupies a part of the ring of

$$\frac{l_b}{C} = \sqrt{\frac{\eta_\omega h \beta^2 \gamma}{2\pi} \frac{A}{Z} \frac{m_p c^2}{e U_{RF}} 2 \frac{\Delta p_{st}}{p}} \approx 0.01, \tag{6.15}$$

where $h = 1$ is the harmonics number.

6.1.4. BETACOOL simulation for the first operation scenario

The BETACOOL code developed by JINR group [9] was especially modified for the numerical simulation of electron cooling in presence of betatron acceleration. The modified code simulates turn by turn a single particle motion inside the storage ring taking into account an action of electron cooling, RF system and induction acceleration. The particle betatron motion is described using the ring transformation matrix of the ring at the position of the electron cooling system. The ion synchrotron motion is simulated by the particle momentum variation after crossing the RF cavity in accordance with the phase and amplitude of RF voltage. The ion velocity variation in the electron cooling system is calculated in accordance

with analytical expressions for the friction force in the magnetized electron beam with flattened velocity distribution [6]. Action of the induction acceleration accounted by the ion momentum variation at each turn in the ring by the value corresponding to the accelerating voltage (6.8). The simulation was performed at the ring and cooling system parameters in the Table 6.1. Initial value of the ion Courant – Snider invariants were taken equal to expected beam emittance after injection. Initial ion momentum shift was chosen equal to the maximum one in the injected beam.

Table 6.1. The parameters of storage ring and ion beam in BETACOOL simulations

Ring circumference, m	110
Ion energy, MeV/u	700
Accelerating betaron voltage, V	150
RF voltage, kV	0.2
Ion beam emittance, π·mm·mrad	1/1
Maximum momentum shift, $\Delta p/p$	$5 \cdot 10^{-3}$
Cooler length, m	3
Beta-function in cooler, m	10/10
Dispersion in cooler, m	0
Electron beam radius, cm	0.5
Electron beam current, A	3
Transverse/ longitudinal electron temperature, meV	100/0.2

Examples of the simulation results for two kind of ions are presented in the Fig. 6.5, 6.6.

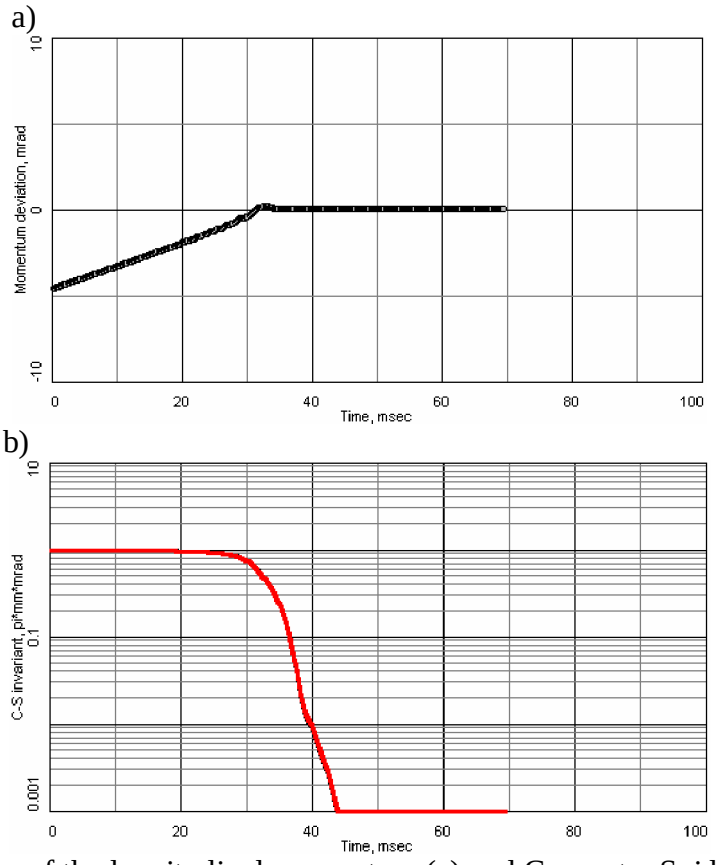

Fig.6.5. Dependence of the longitudinal momentum (a) and Courant – Snider invariant (b) of the $^{200}Pb^{80+}$ ion on time.

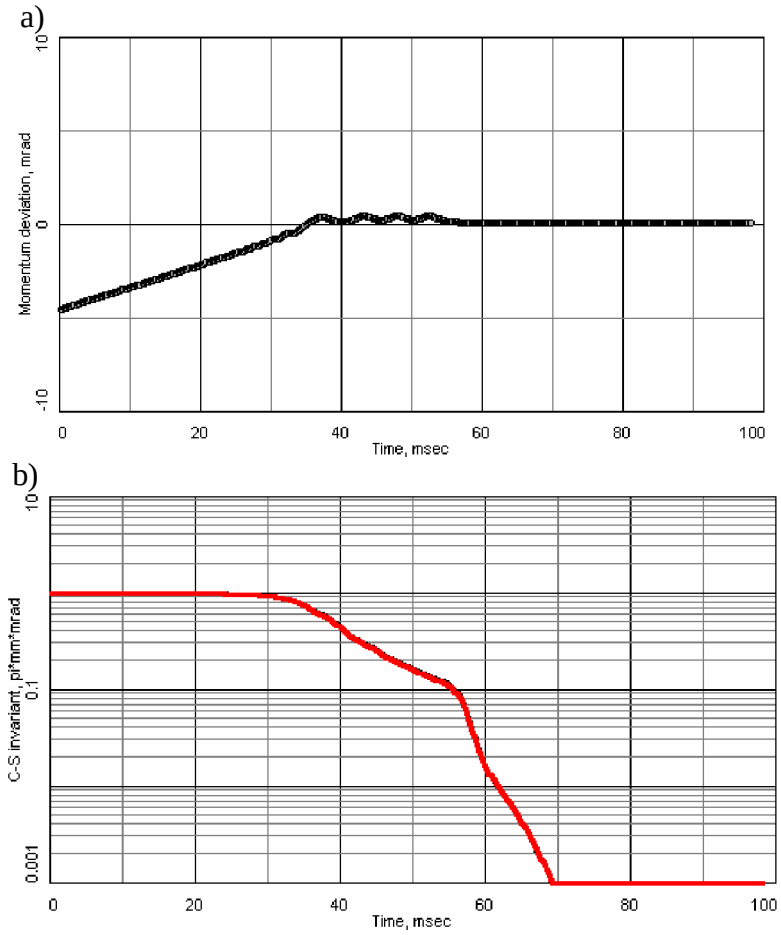

Fig. 6.6. Dependence of the longitudinal momentum (a) and Courant – Snider invariant (b) of the $^{132}Sn^{50+}$ ion on time.

At the initial stage of the stacking process (the first 20 ms in Fig. 6.5 and the first 30 ms in the Fig. 6.6) the electron cooling does not influence on the ion velocity practically (because of a big difference between ion and electron longitudinal velocity) and ion momentum increases due to induction acceleration only. When the ion velocity is sufficiently closed to the electron one the electron cooling begins to work and the ion Courant – Snider invariant decreases very fast. The ion is captured into the separatrix of the synchrotron motion and after a few oscillations (see the interval between 30 and 50 ms in the Fig. 6.6 a) it moves into the stack.

After optimisation of the RF amplitude and induction acceleration voltage one can obtain the stacking time of 35 – 40 ms for each kind of ions. Further decrease of the τ_{acc} value can be achieved by increase of the electron beam density or the cooler length.

6.2. Second operation scenario. Electron cooling with "the gradient electron beam"

6.2.1. General description. Design of the cooling system

In the second ring operation scenario the betatron induction accelerator is unused. The electron cooler is modified in such a way (Fig. 6.7) that the electrons receive a gradient (dispersion) of longitudinal velocities across the electron beam:

$$D_e^{-1} = \frac{1}{p_e}\frac{dp_e}{dx}. \qquad (6.16)$$

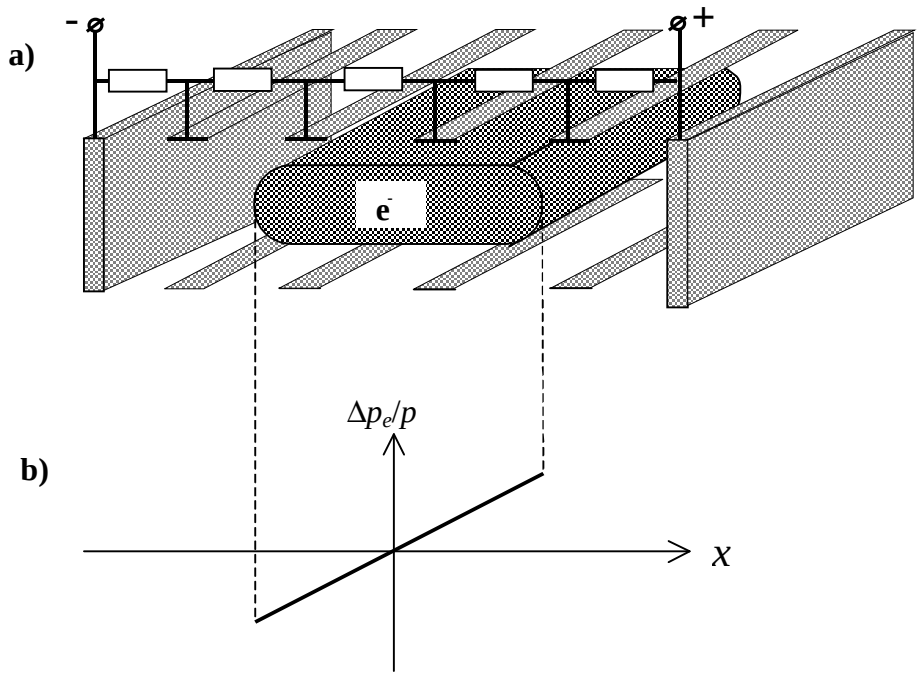

Fig. 6.7. The scheme of the electron cooler with a gradient of longitudinal electron velocity across the beam: a) - the cooling section design, b) – momentum distribution across the beam.

It permits to provide a fast electron cooling of an injected ion independently on its momentum shift comparing with the stack ions. The principle of the cooling with "the gradient electron beam" can be illustrated by the Fig. 6.8.

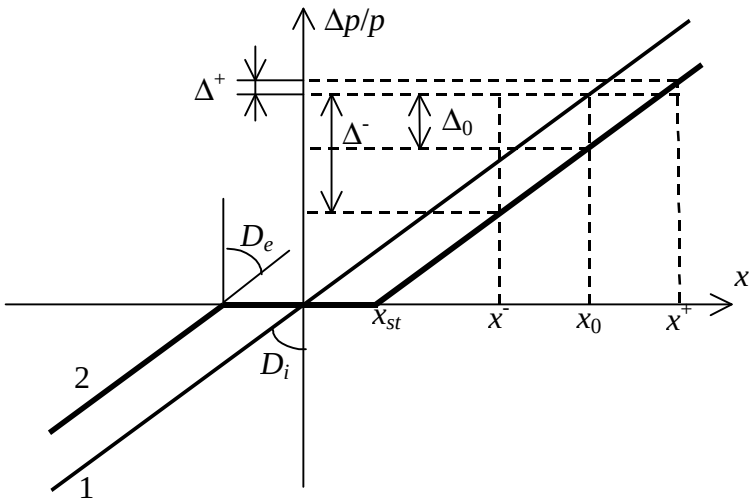

Fig. 6.8. Principle of the cooling with the gradient of the electron velocity.

The electron cooling section is positioned in the ion trajectory place with nonzero dispersion D_i. The straight line 1 in the Fig 6.8 corresponds to the relation between the ion orbit position x_i and the ion momentum shift Δp:

$$x_i = \frac{\Delta p}{p}_i D_i . \tag{6.17}$$

The electron momentum is shifted from nominal value (corresponding to average velocity at $x = 0$) depending on horizontal co-ordinate by the following way (line 2 in the Fig. 6.8):

$$\begin{cases} \frac{\Delta p}{p}_e = \Delta_0 + \frac{x}{D_e}, & x > x_{st} \\ \frac{\Delta p}{p}_e = -\Delta_0 + \frac{x}{D_e}, & x < x_{st} \end{cases}, \tag{6.18}$$

where Δ_0 is some non zero value defined below.

In the case when

$$D_e = D_i \tag{6.19}$$

the ion longitudinal velocity in the electron rest frame v_i in any point x_i is proportional to the Δ_0 value and does not depend on the ion momentum if

$$\left|x_i\right| = \left|\frac{\Delta p}{p}_i\right| D_i > x_{st} . \tag{6.20}$$

Thus the cooling force does not depend on ion momentum in the interval (6.20) and it decelerates the ion, if $\Delta p/p_i > 0$, and accelerates, if $\Delta p/p_i < 0$. Therefore all the ions independently of their momentum are collected near the axis with the constant rate of the momentum variation. The value Δ_0 can be chosen in such a manner, that the ion velocity in the electron rest frame corresponds to maximum of the cooling force value (Formula 6.11).

The picture is more complicated at non zero amplitude of the ion betatron oscillations. In this case the ion position inside the electron beam oscillates from x^- to x^+ (Fig. 6.8):

$$x_0 - x^- = x^+ - x_0 = \sqrt{I_{CS}\beta_x} , \tag{6.21}$$

where I_{CS} is the Courant – Snider invariant of the ion horizontal motion and β_x is the horizontal beta function. The longitudinal ion velocity in the electron rest frame oscillates from the value corresponding to Δ^- to the value corresponding to Δ^+ and even can change a sign. The average value of the cooling force is significantly reduced. This peculiarity is very important for design of the cooling section parameters due to relatively large value of the initial ion beam emittance – of about $\varepsilon_{in} = 1.5\ \pi \cdot mm \cdot mrad.$

Due to complicated dependence of the cooling force on the ion velocity the optimum choice of the dispersion in the cooling section and the Δ_0 value was performed using numerical simulation (see the next Section). However, expected stacking time can be estimated using experimental dependence of the cooling force on the ion velocity (Fig. 6.4). The maximum of the normalised cooling force is about

$$F_{cool}/Z^2 \approx 0.5 \div 1 \text{ eV/m}, \tag{6.22}$$

and for an ion with $Z = 50$ the energy variation after a single crossing of the cooling section of the length of 2 m is about 2.5 ÷ 5 keV. The cooling time at the maximum initial momentum shift of the ion is about 20 ms.

The horizontal dimension of the electron beam has to be larger than

$$x_e = 2D_i \frac{\Delta p}{p}_{i,\max}, \tag{6.23}$$

and at $\Delta p / p_{i,\max}$ of about $2.5 \cdot 10^{-3}$ and dispersion of about 10 m exceeds the value of 5 cm. At such a diameter an electron beam of a round shape of cross-section will have extremely large current. Therefore this scheme presumes a ribbon electron beam, and vertical dimension is determined by initial value of the ion beam emittance:

$$y_e \sim 2\sqrt{\varepsilon_y \beta_y}, \tag{6.24}$$

where β_y is the vertical beta function. At initial beam emittance and β_y of about 10 m the vertical electron beam dimension is less than 1 cm.

Stability of the ribbon electron beam and compensation of different kinds of its drift motion are the main technical problems have to be solved for this scheme realisation.

6.2.2. BETACOOL simulation for second operation scenario

To simulate the cooling process for the second operation scenario using BETACOOL the possibility to vary the electron beam momentum in accordance with line 2 in the Fig. 6.8 was introduced into the code. The numerical simulation was performed at the same general parameters of the ion ring as presented in the Table 6.1. To provide “the gradient cooling” the ring dispersion in cooling section was chosen of $D_i = 16$ m. The electron current density in all the calculations was equal to 0.5 A/cm^2, independent ofy76 the electron beam dimensions. The dispersion of the electron velocity was equal to dispersion of the ring $D_e = D_i$. The value of the parameter Δ_0 (Fig. 6.8) was changed depending on the ion parameters to provide minimum value of the cooling time.

Due to strong dependence of the electron cooling time on the ion energy the calculations were performed in the energy range from 300 MeV/u to 700 MeV/u. Two examples of the cooling process dynamics at different energies are presented in the Fig. 6.9, 6.10. The cooling process consists of three stages. At the first one (the first 15 ms in the Fig. 6.9 and the first 45 ms in the Fig. 6.10) the ion has a large initial Courant – Snider invariant of the horizontal betatron motion. Therefore, longitudinal cooling has a relatively poor efficiency (see explanation in the previous Section). Thereafter, when the Courant –Snider invariant decreases to the value of about 0.2 π·mm·mrad the betatron oscillations do not influence on the longitudinal cooling force and the ion momentum shift decreases very fast. And at the final stage of the cooling process (time interval from about 17 to 23 ms in the Fig. 6.9 and from 45 to 70 ms in the

Fig. 6.10) the ion is captured inside the separatrix and after a few syncrotron oscillations it moves into the stack.

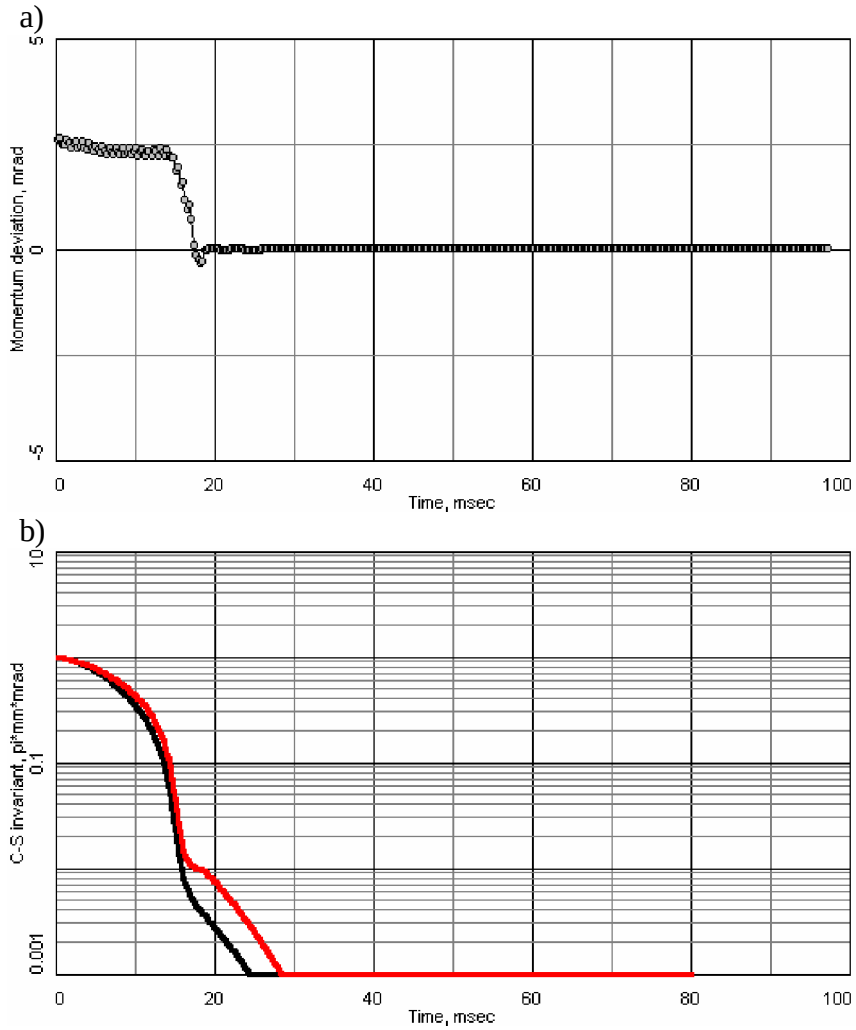

Fig. 6.9. Dependence of the longitudinal momentum (a) and Courant – Snider invariant (b) of the $^{200}Pb^{80+}$ ion on time. The ion energy is 300 MeV/u.

The stacking time for $^{200}Pb^{80+}$ ions corresponds to 23 ms at the ion energy of 300 Mev/u and increases up 70 ms at the ion energy of 600 MeV/u.

These results show, that for second operation scenario a small initial value of the ion beam emittance is very important. For instance without the degrader application in the transfer channel the initial beam emittance corresponds already to the stage of the fast longitudinal cooling. Therefore, the stacking time without the degrader application is almost the same as in the case of the momentum reduction with the degrader. It means, that for the second operation scenario an accurate optimisation of the degrader parameters is necessary. Other way to decrease the stacking duration is an optimization of the dispersion and beta function values of the ring lattice in the cooling section position.

a)

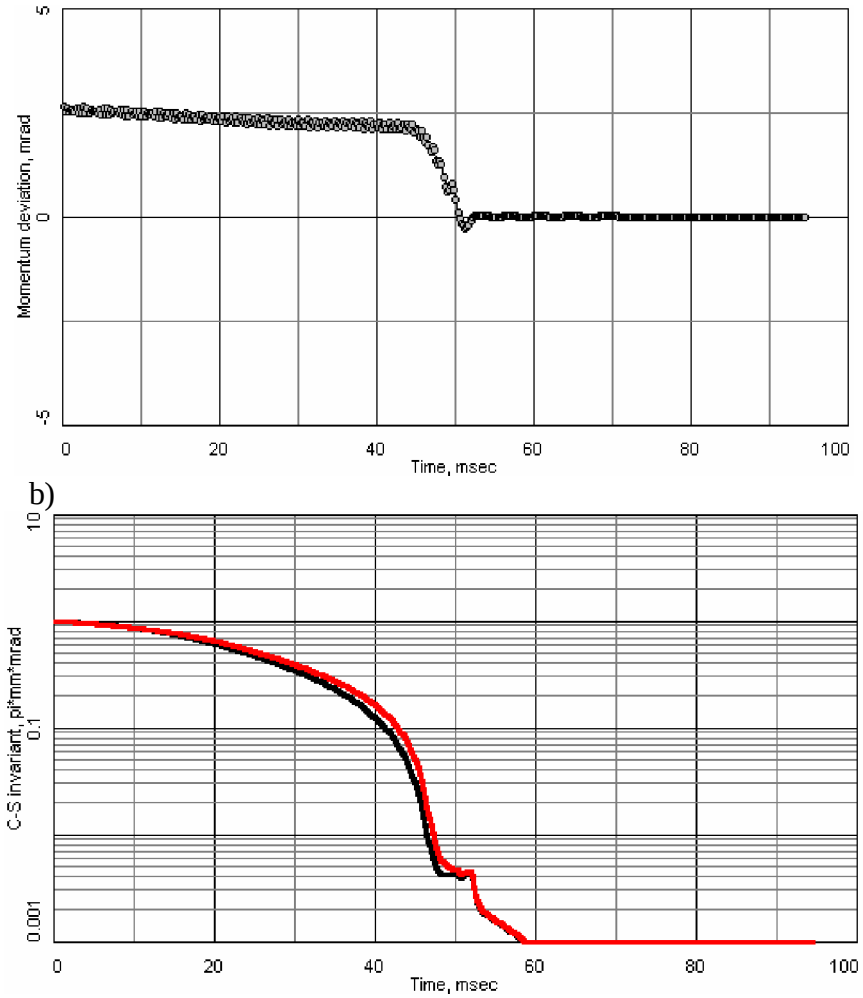

Fig. 6.10. Dependence of the longitudinal momentum (a) and Courant – Snider invariant (b) of the $^{200}Pb^{80+}$ ion on time. The ion energy is 600 MeV/u.

For ions lighter than lead ions (Fig. 6.11) the cooling process has the same peculiarities, but the stacking time is longer due to dependence of the cooling force on the ion parameters as Z^2/A.

Thus, even without optimisation of the transfer line parameters the stacking time of about 30 ms can be obtained for heavy ions at energy values up to 500 MeV/u approximatelly. At larger ion energy one cane hope to obtain such a value after accurate choice of the transfer line and ring parameters. In any case, general limitation of the “gradient electron cooling” application is strong dependence of the cooling efficiency on the ion energy.

The second scenario of the ring operation looks very attractive at the ion energy chosen for MUSES project (about 220 MeV/u). In this case expected stacking time can be less than 10 ms, which is sufficiently less than in both other scenarios. At the ion energy of 700 MeV/u the efficiency of the first and third scenarios can be higher than the second one due to application of induction acceleration and stochastic cooling that depends on the ion energy very week.

a)

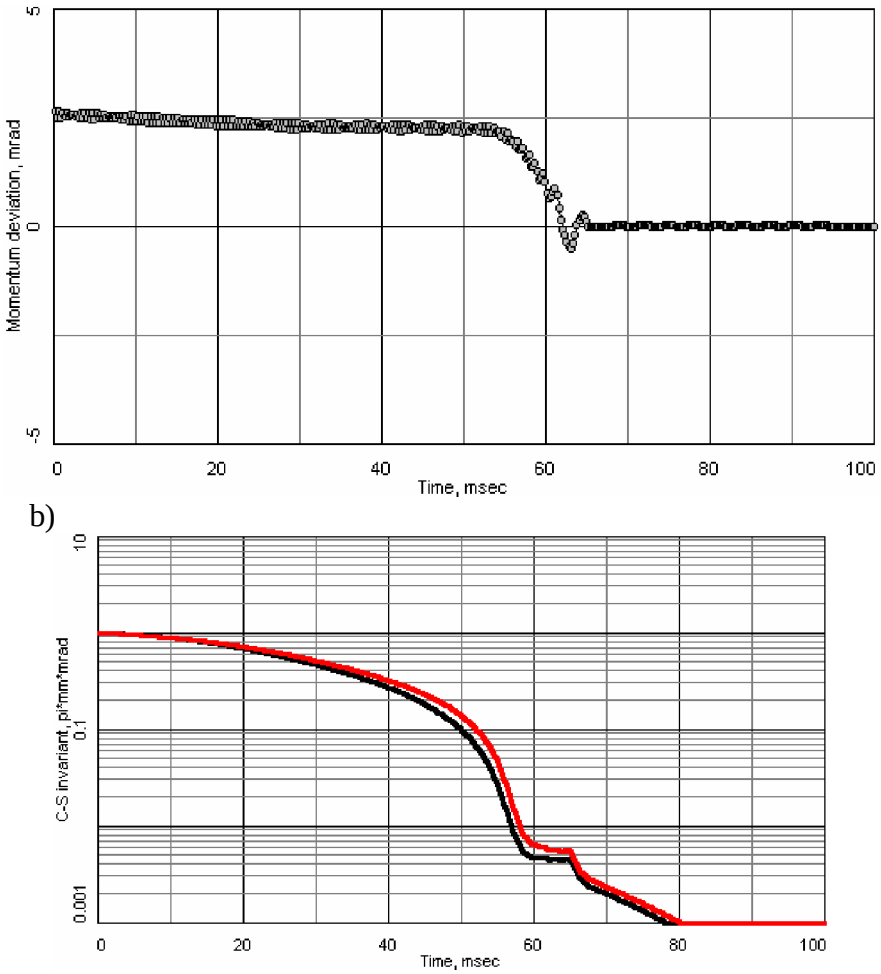

Fig. 6.11. Dependence of the longitudinal momentum (a) and Courant – Snider invariant (b) of the $^{132}Sn^{50+}$ ion on time. The ion energy is 500 MeV/u.

6.3. Third ring operation scenario. Stochastic cooling

At high ion energy the efficiency of stochastic cooling can be significantly higher than electron cooling, and an application of stochastic cooling is desirable for fast cooling at small number of ions in the storage ring. At optimum gain of an amplifier the stochastic cooling time linearly decreases with a decrease of the particles number N in accordance with well-known formula:

$$\tau^{-1}_{cool} \approx \frac{2w}{N}, \tag{6.25}$$

where w is the band width of feed back system. However the optimum gain of the amplifier G_{ampl} increases with a decrease of the particle number and the amplifier output power P_{aml} increases in accordance with the formula [10]:

$$P_{ampl} = \left(T_{ampl} + T_{p-u}\right) \cdot \left(1 + U^{-1}\right) w G_{ampl}{}^{2}, \tag{6.26}$$

where T_{ampl} and T_{p-u} is temperature of amplifier and pick-up electrodes, G_{ampl} is the gain of the amplifier, U is the noise factor given as the noise of the system divided by the beam noise per Schottky band. For instance, at the parameters of the stochastic cooling system proposed for

ACR ring of the MUSES project the optimum amplifier output power at the ion number of about 10^3 exceeds 1 MW for ions of $A \approx 100$ and $Z \approx 50$ (Fig. 6.12).

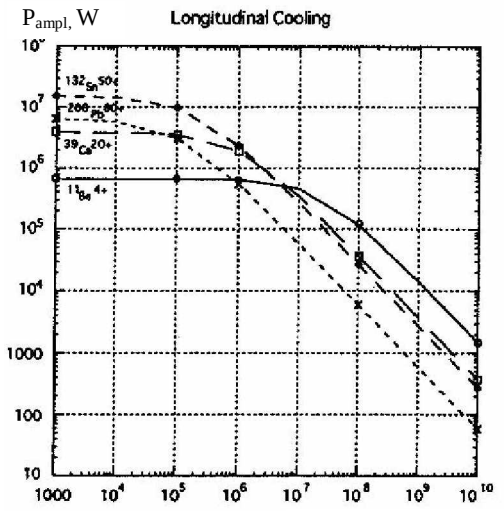

Fig. 6.12. Dependence of the optimum amplifier power on the ion number for different kinds of ions.

At a fixed value of the output amplifier power the cooling time saturates at small number of the ions $N \leq 10^4$. The numerical simulation at ACR cooling system parameters and at 1 kW of the output amplifier power (Fig. 6.13, 6.14) [10] has shown that the longitudinal cooling time for heavy ions saturates at the level of $\tau_{cool} \approx 10$ ms, when the ion number is below 10^4. The transverse cooling time has a closed value: $\tau_{\perp cool} \approx 3ms$.

Thus an application of stochastic cooling permits to provide a sufficiently fast cooling at small ion number. So, a decrease of an initial momentum spread by one order of magnitude requires the time of $2\tau_{cool} \sim 20$ ms about. The third scenario presumes the ion beam bunching after the cooling. The typical time of beam bunching τ_{RF} is approximately equal to ten periods of the ion synchrotron oscillations and can be estimated by the value of 10 ms.

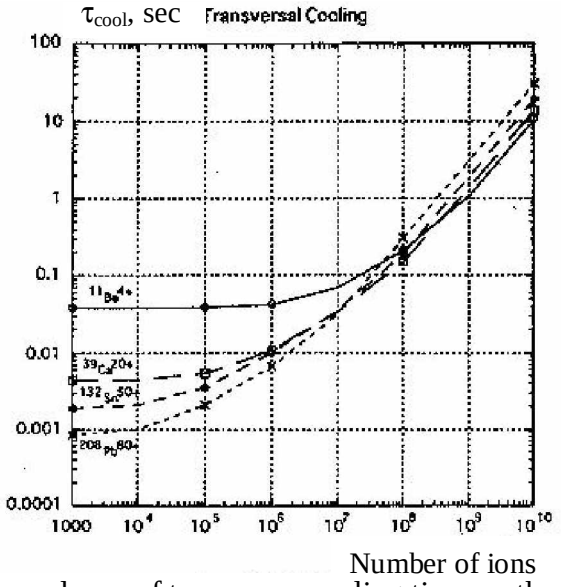

Fig. 6.13. Dependence of transverse cooling time on the ion number.

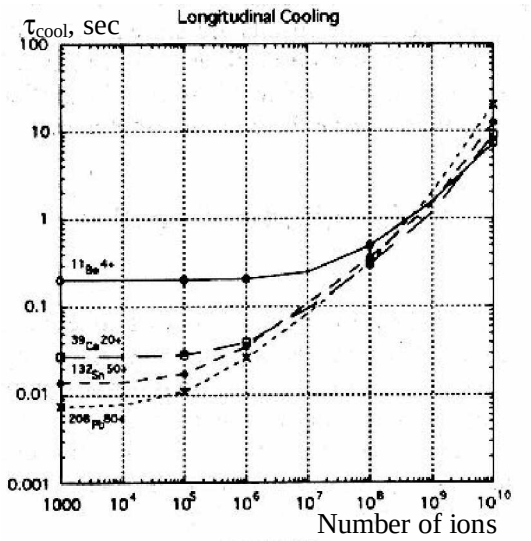

Fig. 6.14. Dependence of the longitudinal cooling time on the ion number.

Finally, the stacking period duration at the second operation scenario is about

$$\tau_{st} = \tau_{cool} + \tau_{RF} \approx 20\text{-}30 \text{ ms}. \qquad (6.27)$$

Conclusion

The scheme of an accelerator facility discussed in this report is based on an individual ion injection, cooling and storage in a ring with a small acceptance. The application of the "individual trajectory correction" in the transfer channel, "individual injection" in the storage ring and fast stacking procedure applied for injected beam at small emittance and momentum spread permits to achieve high storage efficiency for the ions at a low production rate.

After a fragment separator a radioactive ion beam produced at a target bombarded with a primary beam has usually a large emittance of about 200π ·mm·mrad and momentum spread of about ± 2.5%. At low production rate the parameters of each particle can be measured individually with rather high accuracy with a special analyser system. Using a system of kickers (controlled by the analyser) in the transfer channel one can compensate initial ion spatial and angular co-ordinates. The beam emittance at the exit of such a transfer channel is determined by the analyser resolution mainly and can be about $0.2\ \pi$ ·mm·mrad.

In the case, when the ion trajectory is corrected with two kickers in each plane - the horizontal and vertical, the voltage at the first kicker is determined by the beam emittance after fragment separator. At typical ion beam parameters the maximum voltage of the first kicker is about 500 kV. It is evident that a kicker operating at such a voltage and pulse duration of about 30 ns is a very complicated technical installation. In addition the high voltage pulsed generator had to form rectangular pulses of a random distribution in time at a high repetition frequency. Thus the first kicker operation at high repetition frequency is main technical problem of the proposed scheme. In principle, the maximum kicker voltage can be reduced by use of a few kickers or by special kicker design. All the possibilities will be investigated in details at the stage of the transfer channel technical design. In this report for preliminary estimations we assumed that the technically achievable repetition frequency is limited by the value of 10 kHz.

Knowing the moment of an ion generation in the target one can provide an "individual injection" of the ion into a storage ring. The injection is performed by a fast kicker controlled by the signal from analyser system. To avoid losses of ions stacked before the stored beam has to be bunched and the bunch length has to be significantly less than the ring circumference. In this case the injection kicker operation can be synchronised with the bunch revolution. To obtain a short bunch one needs to reduce initial momentum spread of the beam to the value of about 10^{-4}.

Required reduction of the beam momentum spread can be performed, for instance, using longitudinal stochastic cooling. The stochastic cooling application looks reasonable in this case due to small particle number in the ring. At realistic parameters of the cooling system an achievable cooling time value can be about 10 ms. This regime presumes a periodical injection into the ring: after the injection completion the RF system has to be switched off, the ion beam is stochastically cooled down, thereafter the "cooled" coasting beam has to be bunched again. Therefore the stacking time includes also the time required for the beam bunching and the stacking efficiency is reduced by the efficiency of the bunching process.

In the case of an electron cooling application the RF system can work continuously, that simplifies the ring operation and, in principle, can reduce the stacking time. However, at high

initial momentum spread of the ion beam an efficiency of a conventional electron cooling system is poor. This problem can be avoided by two ways.

First of them assumes an application of an induction acceleration for fast ion energy reduction (or increase). In this case, the electron cooling system is used for the stack parameter stabilisation only. Parameters of a betatron core used for induction acceleration are determined by the initial momentum spread of the ion beam. The betatron core dimensions are reasonable if the ion beam momentum spread is less than $5 \cdot 10^3$ approximately. The ion momentum spread after the fragment separator can be reduced to this value using a profile energy degrader in the transfer channel. The beam emittance increases after crossing the degrader. Regular increase of the beam emittance (related to excitation of betatron oscillations in the transfer channel) can be compensated using a second kicker system after the degrader. However, the beam emittance after the second kicker system will be always higher than before crossing the degrader due to stochastic nature of the ion multiscattering process inside the degrader material. Estimations show that the application of the profile energy degrader and two pairs of kickers permits to achieve the beam momentum spread of $\Delta p/p = \pm 2.5 \cdot 10^{-3}$ at emittance of $1.5\ \pi \cdot mm \cdot mrad$ at the exit of the transfer channel. At these parameters the stacking time with induction acceleration can be comparable with the scheme based on stochastic cooling application.

Second possibility of an electron cooling application requires certain modification of the cooling system design. In such a modified electron cooler a ribbon electron beam with transverse (horizontal) gradient of longitudinal electron velocity is used. That permits to provide fast longitudinal cooling of the ions independent of the ion momentum. The fast longitudinal cooling is possible at relatively small emittance value only, therefore the profile energy degrader parameters have to be optimised to obtain minimum stacking time. This scheme of the storage ring looks more attractive than two previous ones due to simplest ring operation. It general limitation is connected with the strong dependence of the electron cooling efficiency on the ion energy. (In the case of induction acceleration application the stacking time is limited by the betatron core parameters mainly and the dependence of the cooling force on the ion energy is not so important.)

The estimations presented in this report show that all three proposed schemes of the storage ring operation allow obtaining comparable stacking time values. The final choice of the ring design will be determined by technical reasons.

The ion storage rate is determined by the ion flux from fragment separator and by the stacking time and the stacking process efficiency. As the estimations presented here have shown, at the individual injection of the ions and fast stacking in the ring the storage rate increases with an increase of the ion flux intensity and reaches the level of $5 \cdot 10^2 \div 10^3$ ions/s when the flux intensity is equal to the kicker repetition frequency (10 kHz). At the ion flux of 10^4 ions/s the storage rate exceeds that one of a scheme based on multiturn injection by about two orders of magnitude. At the ion flux of 10^6 ions/s and higher the storage rate can be increased by about 3 times, i.e. up to a few thousands ions per second, at the same repetition frequency of the kicker operation by synchronisation of the kicker pulses with the ions circulating in the ring.

References

1. P.Bertrand, W. Mittig, P. Roussel-Chomaz Targets for published high intensity beams, to be published

2. K. Blashe, B. Franzke, IV EPAC, London, 1994, p.133

3.Y. Yano, A. Goto, T. Katayama Overview of RIKEN RI Beam Factory Project, Collected Papers of the RIKEN RI Beam Factory Project, Preprint RIKEN, p.1, 1998

4. V. Gorbachev, I. Ivanov, V. Kossoukine et al Transverse damping system for the future CERN LHC, EPAC 2002 to be published

5.D.Dinev Heavy ion injection in synchrotrons and storage rings, Phys. Part. Nucl. 28 (2), 1997, 449

6. I.N. Meshkov Phys. Part. Nucl. 25 (6), 1994, 631

7. H. Danared Electron cooling at CRYRING with an expanded electron beam, NIM A391, 1997, 24

8. N.S. Dikansky, V.V. Parhomchuk et al. Ultimate possibilities of electron cooling, Preprint BINP №

9. I .N. Meshkov, A. Smirnov, A. Sidorin et al Application of BETACOOL code for dynamic of ions in a storage ring, ECOOL01, Germany, 2001

10. N.Inabe, K. Yoshida, M. Wakasugi and T.Katayama, Study of Stochastic cooling at ACR, Collected Papers of the RIKEN RI Beam Factory Project, Preprint RIKEN, p.88, 1998